THE BOREHOLE-FLUID EFFECT IN ERT

Published in *Geophysics*:

Doetsch, J. A., Coscia, I., Greenhalgh, S., Linde, N., Green, A., and Günther, T., 2010. The borehole-fluid effect in electrical resistivity imaging, *Geophysics,* **75**, F107-F114.

ABSTRACT

Fluid that fills boreholes in crosswell electrical-resistivity investigations provides the necessary electrical contact between the electrodes and the rock formation, but it is also the source of image artifacts in standard inversions that do not account for the effects of the boreholes. The image distortions can be severe for large resistivity contrasts between the rock formation and borehole fluid and for large borehole diameters. We have carried out 3-D finite-element modeling using an unstructured-grid approach to quantify the magnitude of borehole effects for different resistivity contrasts, borehole diameters, and electrode configurations. Relatively common resistivity contrasts of 100 : 1 and borehole diameters of 10 and 20 cm yielded, for a bipole length 5 m, apparent resistivity underestimates of approximately 12% and 32% when using AB-MN configurations and apparent resistivity overestimates approximately 24% and 95% when using AM-BN configurations. Effects are generally more severe at shorter bipole spacings. We report here the results obtained by either including or ignoring the boreholes in inversions of 3-D field data from a test site in Switzerland, where approximately 10,000 crosswell resistivity tomography measurements were made across six acquisition planes between four boreholes. Inversions of raw data that ignored the boreholes filled with low resistivity fluid paradoxically produced high resistivity artifacts around the boreholes. Including correction factors based on the modeling results for a 1-D model with and without the boreholes did not markedly improve the images. The only satisfactory approach was to use a 3-D inversion code that explicitly incorporated the boreholes in the actual inversion. This new approach yielded an electrical resistivity image that was devoid of artifacts around the boreholes and that correlated well with co-incident crosswell radar images.

1.1 INTRODUCTION

Crosswell and borehole-to-surface electrical resistance tomography (ERT) is a popular and powerful method of subsurface imaging in engineering and environmental investigations [*LaBrecque et al.*, 1996a; *Slater et al.*, 2000; *Linde et al.*, 2006a; *Wilkinson et al.*, 2010 and references contained therein]. The boreholes used for such ERT investigations are usually partially filled with water, either naturally if below the water table or artificially if measurements are made in the unsaturated zone. The water provides electrical contact between the suspended electrode string and the surrounding rock formation (i.e., the rock matrix with its associated pore-filling fluids). Other methods of installing the electrodes less

common but still provide adequate electrode coupling. For example, electrodes can be mounted on the outside of a PVC tube that is lowered down the well and held in firm contact with the borehole wall (mandatory in air-filled holes), or the borehole can be back-filled with mud or moist sand after the electrode string is deployed.

In most common near-surface geological settings, the rock has a higher electrical resistivity than its contained fluid [*Keller and Frischknecht*, 1966]. Regardless of the method of electrical contact used (fluid-filled or soil-filled holes), there is usually a substantial contrast between the resistivity of the rock formation ρ_r and that of the borehole fluid ρ_f. This contrast usually results in a narrow cylindrical conductive anomaly that influences the ERT measurements. The current from a borehole source will preferentially flow within the more conductive fluid rather than out into the rock. The $\rho_r : \rho_f$ contrast, and hence the associated borehole effect on ERT measurements, will be particularly large if the borehole is filled with saline fluid or clay and the host material is hard rock. In a later section of this paper we investigate an ERT field example involving a saturated gravel aquifer. Using Archie's law [*Archie*, 1942], and assuming a porosity of 0.25, a cementation factor of 1.5, and the same salinity water in the borehole as in the pore space of the rock, the expected resistivity contrast $\rho_r : \rho_f$ between the saturated gravel and water-filled borehole is about 8 : 1. Even such a modest contrast has a significant effect on the cross-hole apparent resistivities. It should be remarked that a resistive air-filled borehole also constitutes a 3-D anomalous structure that will affect the measurements (when electrodes are held in direct contact with the formation), but not as severely as in the conductive case.

The borehole fluid effect is well known in electric-well logging, in which the influence of not only the borehole fluid but also that of the mud cake and mud filtrate surrounding the borehole are taken into account [*Darling*, 2005]. Special focused well-logging resistivity tools incorporate additional guard electrodes to force the current to flow radially outwards into the formation, rather than axially within the conductive fluid.

In ERT investigations, the borehole effect is rarely considered. Data are generally inverted and interpreted without due account for the resistivity contrast between the rock formation and borehole fluid. Yet, a number of studies [*Daily and Ramirez*, 1995; *Osiensky et al.*, 2004; *Daily et al.*, 2005; *Nimmer et al.*, 2008] have demonstrated that this approach can produce serious artifacts (i.e., fictitious features in the inverted resistivity images). One reason why this effect is often ignored in crosswell ERT is that to adequately incorporate the boreholes in both the forward modeling and inversion codes requires a 3-D representation of

the subsurface that allows the narrow boreholes and adjacent regions to be very densely meshed. This can only be achieved satisfactorily with an unstructured finite-element mesh, such as described by *Rücker et al.,* [2006], *Günther et al.* [2006], and *Blome et al.* [2009]. Most ERT forward modeling and inversion codes are based on structured (regular) grids or meshes that cannot adequately or efficiently represent boreholes, particularly when they deviate from the vertical or horizontal. With structured meshes, it is computationally prohibitive to use very fine grids, especially in 3-D. As a consequence, most ERT reconstructions are based on 2.5-D modeling that treats the boreholes (if at all) as infinite sheets (2-D structures) rather than as cylinders (3-D structures).

By means of a regular 3-D finite-difference modeling approach, *Osiensky et al.* [2004] compute the equipotential pattern surrounding a current source placed at the bottom of a square borehole located within a homogeneous rock formation. They present results for the borehole being either fully air-filled (i.e., more resistive than the host formation) or partially liquid-filled with fresh or saline water (i.e., more conductive than the host formation). The air-filled hole yields quasi-circular equipotential contours, whereas in the case of a conductive fluid the equipotentials are more elliptical and elongated in the direction of the borehole. The ellipticity increases with the resistivity contrast. Voltage levels in the rock formation differ substantially for the two cases (air-filled versus saline-fluid-filled) in the near-vicinity of the borehole, but the equipotentials appear quite similar in shape and magnitude at a distance of two to three times the borehole depth. *Osiensky et al.* [2004] suggest that failure to consider this "noise" in crosswell or borehole-to-surface measurements can lead to incorrect interpretations of the apparent resistivities.

Nimmer at al. [2008] used a structured finite-element method (FEM) approach to numerically compute the spatial variations of voltage ratio for a downhole current electrode in either an air-filled or a partially liquid-filled borehole. The ratio was taken relative to the situation of no borehole at all (i.e., current electrodes buried in a half-space). They show that the increased current density in the liquid-filled borehole results in lower current density in the formation and therefore anomalously reduced voltages (i.e., ratios of < 1). Conversely, the air-filled hole results in slightly higher voltages in the formation (i.e., increased current density) due to the resistive cylinder. They also present inversion results for synthetic tomography experiments involving roving bipoles of 3 m length in two 15-m-deep boreholes placed 10 m apart. Each 10 × 10 cm square borehole, which is represented by a regular FEM grid of 2 × 2 × 30 cells, is occupied by 16 electrodes. *Nimmer at al.* [2008] consider $\rho_r : \rho_f$

values of 10 : 1 and 100 : 1. Inversion results based on the lower contrast differ little from those obtained for a medium without boreholes (i.e., current electrodes buried in a half-space), whereas the results based on the higher contrast contain significant artifacts. They repeated the experiments for 20 × 20 cm square boreholes (using four times as many cells to represent each borehole) and found the artifacts to intensify. The image discrepancy compared to the no-borehole case was a consequence of the inversion algorithm trying to compensate for increased current density in the liquid-filled borehole.

Nimmer et al. [2008] caution against ignoring the borehole-fluid effect whenever the distances involved are small, when the borehole diameters exceed 20 cm, or when the $\rho_r : \rho_f$ approaches $100 : 1$. In such situations they recommend measuring the borehole fluid resistivity and incorporating it in the forward modeling as part of the inversion. However, they suggest that the borehole effects are far less severe in time-lapse tomography investigations, such that they can possibly be ignored if the ratios of voltage (or apparent resistivity) data acquired at different times are inverted, rather than the individual data sets themselves. In this way, the problem of creating biased time-lapse inversion results is effectively hidden.

In this contribution, we demonstrate that accurate forward modeling using a singularity removal technique for the borehole sources and an unstructured mesh for representing narrow boreholes are essential for reliable inversions of crosswell-ERT data. Our study differs from that of *Nimmer et al.* [2008] in that we (1) only consider borehole-related artifacts in the forward modeling of a homogeneous half-space and not other models, (2) consider a wider range of bipole electrode configurations, (3) invert an extensive field data set rather than a synthetic one, and (4) explore the possibility of eliminating the borehole-fluid effects from the apparent resistivity data by calculating and applying correction factors.

After describing the homogeneous model, assumed borehole geometry, and very brief details on the computer code, we present simulated apparent resistivities and related statistics for a range of $\rho_r : \rho_f$ ratios, borehole diameters, electrode configurations, and bipole separations. We then introduce our observed 3-D crosswell-ERT data [*Coscia et al.*, 2010] and show, for the very first time, the results of inverting data with the boreholes explicitly included. For comparison, we also show the results of inverting the data without accounting for the boreholes (i.e., the common practice in crosswell-ERT experiments). In an attempt to minimize the computational effort, we next examine whether correction factors based on

forward modeling studies enable corrected data to be inverted without the need to include the boreholes in the models.

1.2 MODELING THE BOREHOLE-FLUID EFFECT

To investigate the borehole-fluid effect, we used a 100-Ωm homogeneous half-space model penetrated by two 10-m-deep vertical boreholes separated by 5 m (Figure 4.1). This geometry matched that of the crosswell-ERT experiment at our field test site described later in the paper. Modeling was performed for borehole diameters of 5, 10, and 20 cm and various resistivities of the borehole fluid, such that the $\rho_r : \rho_f$ contrasts ranged from 1 : 1 to 600 : 1. Depending on the objectives of the simulation, electrodes were placed at regular intervals of 0.25 or 1 m along the length of each borehole. Two basic recording configurations were simulated (Figure 4.1). Either both current electrodes A and B were placed in one hole and both potential electrodes M and N were located in the other hole (i.e., the so-called AB-MN configurations) or the current electrodes were placed in separate holes, as were the potential electrodes (i.e., the so-called AM-BN configurations). The spacings between the active electrodes were varied from 1 to 9 m.

The modeling is carried out with the versatile 3-D FEM library DCFEMLIB [*Rücker et al.*, 2006], which uses an unstructured finite-element mesh. To achieve sufficient accuracy, a singularity removal technique [*Lowry et al.*, 1989] was used to accommodate the rapid decay of electric potential around each point source position and a high density of elements is automatically meshed around the boreholes (Figure 4.2). The singular potential can be calculated either analytically for homogeneous flat-topography models or numerically using a boundary-element method when surface topography is significant. The singular potential is based on the true resistivity at the point source position (i.e., the borehole-fluid resistivity). The non-singular potential is then computed numerically by the finite-element method. Details on the procedure are given by *Rücker et al.* [2006] and *Blome et al.* [2009]. Final results are presented as apparent resistivities.

We begin by examining apparent resistivity distributions for the three borehole diameters, each $\rho_r : \rho_f$ contrast considered, and all possible recording configurations of the AB-MN and AM-BN types (with electrode spacings incremented progressively by 1 m). If the borehole-fluid effect is negligible, then the apparent resistivities would equal the true 100 Ωm resistivity, such that differences from 100 Ωm are a measure of the borehole-fluid effect. Figure 4.3 shows, in a simplified frequency-polygon form, illustrative data corresponding to a

contrast $\rho_r : \rho_f$ equal to 10 : 1. The spread of apparent resistivities around the true rock-formation resistivity of 100 Ωm increases with increasing borehole diameter. Even for this narrow borehole-diameter, the variation in values is significant (of the order of 10%) at this modest resistivity contrast. The discrepancies grow to 40% for the large diameter case. Clearly, some recording geometries are more sensitive to the borehole-fluid effect than others, as indicated by the outliers on the frequency polygon plot. The variations become larger as the resistivity contrast increases (not shown). We found that the apparent resistivities can become negative for certain asymmetric AB-MN configurations. Negative apparent resistivities are neither uncommon nor unphysical and have been reported in previous studies [e.g., *Marescot et al.*, 2006; *Jung et al.*, 2009].

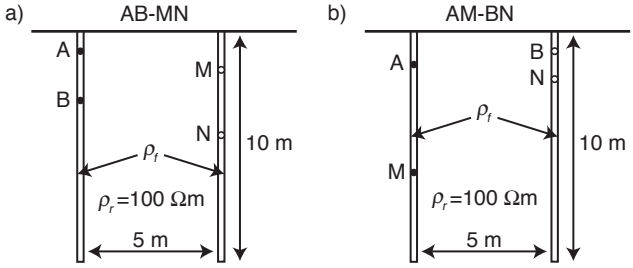

Figure 4.1. Model and crosswell recording geometries used in computing synthetic borehole responses. (a) AB-MN configuration: both current electrodes in one hole and both potential electrodes in the other. (b) AM-BN configuration: each hole contains one current electrode and one potential electrode.

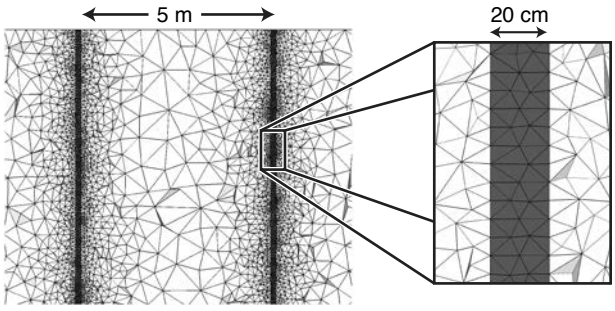

Figure 4.2. Typical unstructured mesh used to represent the subsurface within, around, and between boreholes in a crosswell-ERT experiment.

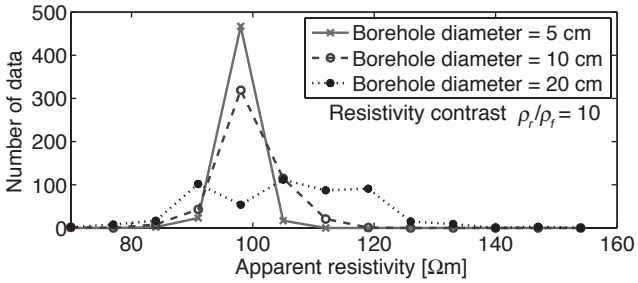

Figure 4.3. Frequency polygons of apparent resistivities obtained for all possible recording configurations (i.e., all combinations of A, B, M, and N electrode depths) and $\rho_r : \rho_f$ = 10 : 1. The three curves correspond to borehole diameters 5, 10, and 20 cm.

Figure 4.4 shows apparent resistivities for electrodes at fixed depths of 1 m and 6 m in both boreholes and varying $\rho_r : \rho_f$ contrasts. The 5 m bipole length and 5 m hole separation equate to 25 times the largest borehole diameter that we tested. The borehole-fluid effect produces anomalously low apparent resistivities for the AB-MN configurations (Figure 4.4a), which means that the voltages are smaller than if the boreholes were not present. The effect is substantial (i.e., apparent resistivities too low by up to 80 %) for large resistivity contrasts and large borehole diameters. Even for $\rho_r : \rho_f$ contrasts of just 100, the effects are ~12% and ~32% for the 10 and 20 cm borehole diameters. The reason for the decrease in apparent resistivity over the no-borehole situation is that current density is increased in the source borehole and reduced elsewhere, including within the borehole containing the potential electrodes. Since the measured voltage is proportional to both the current density and the true resistivity in the immediate vicinity of the potential electrodes, having the potential electrodes in the low resistivity borehole fluid remote from the current source and sink results in anomalously low voltages and hence anomalously low apparent resistivities.

For the AM-BN configurations (Figure 4.4b), the apparent resistivities are anomalously high relative to the no-borehole situation. For a $\rho_r : \rho_f$ contrast of 100, the effects are ~24% and ~95% for the 10 and 20 cm borehole diameters, markedly higher deviations than for the AB-MN configurations. The reason for the increase in apparent resistivity is that each potential electrode shares the same hole as either the current source or the current sink where current density is increased because of the conductive fluid. The increase in current density overwhelms the effect of the low resistivity of the borehole fluid, such that it is sensed by the potential electrodes as anomalously high voltages and apparent resistivities.

Plots of apparent resistivity versus bipole size for a 10-cm borehole diameter and a resistivity contrast of $30 : 1$ are displayed in Figure 4.5 for the AB-MN and AM-BN configurations; an electrode spacing of 0.25 m was used to generate these plots. The bipoles were centered at the midpoint of the holes and their common sizes were varied. This Figure reveals that the borehole-fluid effect increases with decreasing bipole size (AB, MN, AM, and BN). It is more pronounced for the AM-BN configurations, with apparent resistivities anomalous by as much as 36 % for a bipole spacing of 1 m. We also examined the influence of bipole-midpoint depth in each hole. There is essentially no difference (not shown) for symmetric configurations, as in normal scanning where each bipole is at the same depth, but there are effects associated with the bottom and top of each hole. For asymmetric configurations, in which the two bipoles do not share the same depth, the pattern is fairly

stable for AM-BN configurations but erratic for AB-MN configurations, with negative apparent resistivities appearing when the depth difference between the two bipoles exceeds half the borehole depth. This means that the AB-MN configurations can produce singularities in the geometric K factor, which is defined as $K = \frac{4\pi}{\frac{1}{AM} + \frac{1}{A'M} - \frac{1}{AN} - \frac{1}{A'N} - \frac{1}{BM} - \frac{1}{B'M} + \frac{1}{BN} + \frac{1}{B'N}}$ and is thus a function of the distances between the potential electrodes M and N, and the true underground sources A and B as well as the above ground mirror image sources A' and B' [*Günther*, 2004, page 45]. Physically this means that the voltage differences are very small (i.e., potential electrodes lie close to the same equipotential surface) and can even change sign.

The information contained in Figures 4.3 - 4.5 together with the results of earlier synthetic studies by *Osiensky et al.* [2004] and *Nimmer et al.* [2008] demonstrate that apparent resistivities in crosswell-ERT experiments are significantly influenced by the borehole fluid. Unless the effects of the borehole fluids are accounted for, either by explicitly including the boreholes in the finite-element mesh or possibly by applying correction factors to the raw data, regularized tomographic inversions are likely to yield images contaminated with artifacts. Some of the artifacts will be obvious (e.g., anomalous features along the lengths of the boreholes), whereas others may not be easy to identify. In the following, we explore both approaches for handling the borehole-fluid effect, namely: (1) explicitly including the boreholes in the computational mesh, and (2) determining correction factors that can be applied to the raw data, so that the boreholes can be ignored in the inversion process.

1.3 MULTI-HOLE 3-D ERT DATA SET

As part of a multidisciplinary effort to map changing aquifer conditions associated with flood events in an adjacent river, we have recorded a large number of crosswell-ERT data sets at a test site in Switzerland. The geology at this location includes a 3-m-thick surface layer of alluvial sandy loam successively underlain by 1 m of unsaturated gravel, 6 m of water-saturated gravel, and lacustrine clay of considerable thickness. The electrical characteristics are listed in Table 4.1.

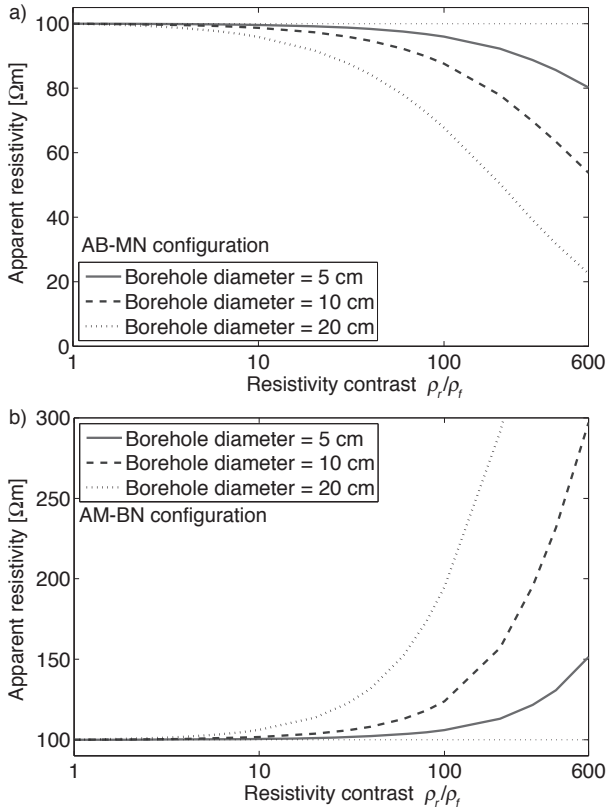

Figure 4.4. Apparent resistivity as a function of $\rho_r : \rho_f$ contrast (log scale) for electrode configurations (a) AB-MN and (b) AM-BN (see Figure 1). Depths to the upper and lower electrodes are kept constant at 1 and 6 m. The three curves shown in each diagram correspond to borehole diameters of 5, 10, and 20 cm.

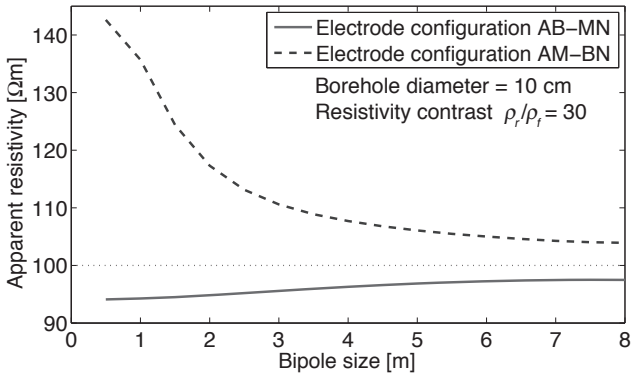

Figure 4.5. Apparent resistivity versus bipole length (the same in each borehole) for a 10 cm borehole diameter and $\rho_r : \rho_f$ = 30 : 1. The bipoles are centered at a depth of 5 m in each hole. Results are given for the two recording configurations AB-MN and AM-BN.

Table 4.1. Layered (1D) model at the test site.

Unit	Thickness [m]	Resistivity [Ωm]
Loam	3	40
Unsaturated gravel	1	1000
Saturated gravel	6	250
Clay	>	20

During a period of stable hydrological conditions when no flood events occurred (and thus no temporal changes in electrical properties of the subsurface), we acquired one large 3-D crosswell-ERT data set using four vertical boreholes located at the corners of a 5 x 5 m square. The 11.4-cm-diameter boreholes penetrated the entire geological section down to the upper part of the clay-rich aquitard. Ten electrodes equally spaced at 0.7 m intervals were installed along the screened part of each borehole that passed through the gravel aquifer. At the time of the experiment, 9 of the electrodes were located within the water-saturated part of the aquifer. The primary purpose of this experiment was to define resistivity variations within the water-saturated part of the aquifer and to investigate the resolving capabilities of different electrode configurations. Complementary crosswell radar and seismic experiments were carried out between the same boreholes over the same depth range for hydrogeophysical characterization of the aquifer (see Chapter 2).

Electrodes within the saturated zone of the gravel aquifer were used to give 3-D coverage across the six possible acquisition planes provided by the 4 boreholes (see sketches at the top of Figure 4.6). Of the 10,224 electrode combinations we employed, 2,464 configurations were of the AB-MN type and 7,760 configurations were of the AM-BN type. The recording instrument allows the repeatability of each voltage reading to be determined from multiple measurements over each current cycle. Data having measurement deviations of more than 1% were eliminated, reducing the data set to 10,035 measurements. We also eliminated potentially noisy data acquired with electrode configurations distinguished by geometric K factors > 1000; in fact electrode configurations with high K factors usually have low signal levels, because the two potential electrodes are close to the same equipotential contour. The remaining 9,203 raw measurements formed the full dataset.

Although it is possible to invert data sets with >9000 values, it is relatively time-consuming. For this reason, we employed an optimized experimental-design procedure to reduce the number of values without significantly reducing the resolution capabilities of the data set. The sensitivities for each electrode configuration were first calculated using a 4-layered earth model (Table 4.1) derived from previously acquired surface- and crosswell-ERT data. The rows of the Jacobian matrix of sensitivities, each one corresponding to a particular configuration, were then compared and used in an optimized experimental-design procedure. Those configurations having the greatest degree of linear independence were added to the base set of 1,000 most sensitive combinations. Details about this optimization approach are described by *Stummer et al.* [2004] and *Coscia et al.* [2008]. In this way, we selected the

5,000 most independent measurements. Our inversions were based on this reduced data set of 5,000 measurements.

1.4 3-D INVERSION RESULTS WITH AND WITHOUT BOREHOLES

We first inverted the 3-D data set using the BERT code [*Günther et al.*, 2006], with an unstructured mesh that incorporated an adequate representation of the boreholes. Each borehole was treated as an independent inversion region with spatial regularization five times stronger than for other inversion regions, but there were no assumptions regarding the electrical resistivity of the borehole fluid (for a discussion on region constraints, see *Günther and Rücker* [2009]). Although the active electrodes were limited to the water-saturated part of the gravel aquifer, the resistivities of the overlying and underlying units as well as the resistivities of immediately adjacent regions outside the cuboid defined by the boreholes will influence the inversion results [*Maurer and Friedel*, 2006]. Accordingly, the inversion domain was defined to be a cuboid of 10 × 10 m horizontal extent and 13.0 m depth.

For reliable and consistent inversion results, it was necessary to decouple the smoothness constraints between the different layers, separating the unsaturated zone and the clay layer from the principal zone of interest. The boundaries at the top and bottom of the saturated zone were known to be sharp, such that smoothing across such boundaries can introduce spurious features. It was therefore important to preserve the abrupt nature of the known lithological and hydrological boundaries (based on the borehole geological logs) to allow subtle but important 3-D variations in resistivity within the gravel aquifer to be mapped. Inversions in which the sharp boundaries were not enforced yielded highly variable and unrealistic resistivities within the aquifer. By adopting this inversion approach, data misfit at the 3 - 4% error level was achieved after four iterations. The starting model for the inversions was a 1-D layered sequence (Table 4.1), based on the average resistivities determined from surface ERT and borehole logs.

Results of the inversion are depicted in 3-D perspective view in Figure 4.6a and b for the 4 outer observation planes. To take advantage of the full color spectrum to represent the relatively narrow but significant 100 - 270 Ωm range of resistivities in the water-saturated aquifer (the primary target of our investigations), the results for the overlying and underlying layers are not presented in Figure 4.6. The inverted values for the lumped loam-unsaturated zone are in excess of 500 Ωm and those for the clay are less than 50 Ωm. The former are consistent with results from companion surface ERT surveys, which yielded values of 60 Ωm

for the loam and approximately 1000 Ωm for the unsaturated gravel. Figure 4.6a and b reveal quasi-subhorizontal resistivity layering near three of the boreholes and a rather diffuse relatively high resistivity feature near the fourth borehole. The resistivity of the borehole fluid has an average value of 27 Ωm, only eight times lower than the average for the rock formation.

Figure 4.6c and d show results of the unstructured BERT inversion with layer decoupling of the gravel-clay and the saturated-unsaturated gravel interfaces, but completely ignoring the boreholes (i.e., by not including them in the mesh generation). Even though the data misfit is similar to runs that included the boreholes, this image is visually different to Figure 4.6a and b; the correlation coefficient between the log resistivities in the two models across the six borehole planes is 0.88. This coefficient might at first sight seem rather high but it should be appreciated that the actual resistivity variations in the aquifer are quite small, and the differences are further compressed when taking logarithms. The quasi-subhorizontal resistivity layering seen in Figure 4.6a and b is not evident in Figure 4.6c and d. Paradoxically, artificial high resistivity zones have been introduced at and around the borehole locations, where in fact the resistivities are low. This is a consequence of the majority of measured apparent resistivities being of the AM-BN type, which have anomalously high values because of the increased current density within the borehole fluid (Figure 4.4b). When the boreholes are not taken into account, the inversion algorithm cannot differentiate whether an increased voltage is due to an increase in current density or an increase in ground resistivity.

We have compared the two 3-D ERT models in Figure 4.6 with the coincident but independently derived 3-D radar and seismic velocity models in Chapter 2. There is excellent correspondence between the resistivity pattern depicted in Figure 4.6a and b and the radar and seismic velocity patterns. The quasi-subhorizontal layering near three of the boreholes and the diffuse feature near the fourth borehole are characteristics of all three 3-D tomograms. We can quantify the correlations. For example, since electrical resistivities likely decrease and radar permittivities likely increase with increased porosity within the saturated gravel, we expect these two parameters to be strongly anti-correlated in the region of interest (even though spatial variations of clay content will probably decrease this anti-correlation). Cross-correlations of the radar permittivity model with the resistivity models based on the ERT inversions with and without the boreholes yield correlation coefficients of -0.66 and -0.52, demonstrating that the ERT inversion with boreholes produces a model that corresponds more

closely to the radar permittivity model than that produced by the inversion that ignores them. These results indicate that the model that ignores the borehole is of limited value to make inferences about internal lithological variations within the gravel aquifer.

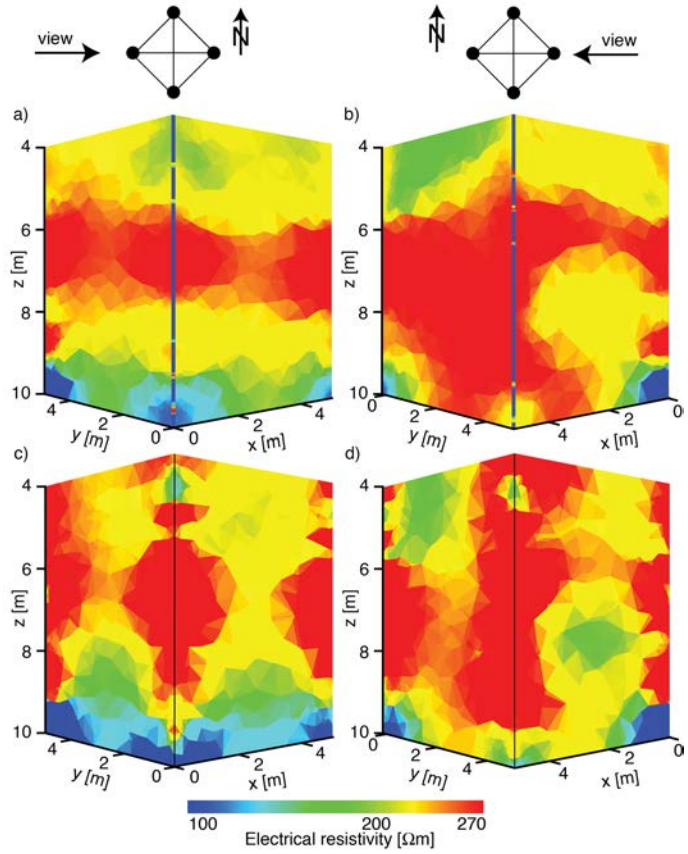

Figure 4.6. Crosswell-ERT data were acquired between 4 boreholes located at the corners of a 5 x 5 m square (a total of 6 planes; see sketches at the top) and inverted using the program BERT with an unstructured mesh. (a) and (b) Two perspective views of a model derived from a 3-D inversion that explicitly incorporates the boreholes (the outer 4 planes are shown). (c) and (d) Corresponding views for a 3-D inversion that did not incorporate the boreholes. Note the high resistivity artifacts along the boreholes in (c) and (d). Note that the color bar is clipped at each end so that any resistivities lower than 100 Ωm remains blue and any resistivity higher than 270 Ωm remains red. The actual recovered borehole resistivity is 27 Ωm.

1.5 THE INADEQUACY OF CORRECTION FACTORS

To avoid the extra computational effort and sophistication that results from including the boreholes in the finite-element meshes, we now investigate the possibility of calculating and applying borehole-fluid correction factors to the data prior to inversion. If this approach proves to be viable, standard schemes based on structured meshes that do not incorporate the boreholes could be used to invert the corrected crosswell-ERT data. We determine the first

suite of correction factors by applying the forward component of the BERT software to the 1-D layered model shown in Table 4.1 with the boreholes and then without the boreholes. The correction factors are the ratios of apparent resistivities from the two forward modeling runs. They are shown in frequency polygon form by the dashed line in Figure 4.7 for the various electrode configurations. The values range from 0.7 to 1.15.

These correction factors were applied to the observed apparent resistivity data and the corrected data were then inverted using the BERT code and an unstructured mesh that ignored the boreholes. The inverted model shown in Figure 4.8a and b is quite different to both the model obtained incorporating the boreholes (Figure 4.6a and b) and the one obtained without applying correction factors (Figure 4.6c and d). The correlation coefficient between this model and the model that explicitly incorporates the boreholes is 0.93. The artifacts along the boreholes in Figure 4.8a and b are not as pronounced as in Figure 4.6c and d, but they are sufficiently strong to obscure the pattern of resistivities between the boreholes. This result clearly shows that corrections based on a layered model are inadequate for this data set.

We repeated the calculation and application of correction factors, but this time we replaced the 1-D model (Table 4.1) with the final 3-D model of Figure 4.6a and b. The distribution of these correction factors is shown by the solid line in Figure 4.7. The shape of this histogram is notably different from that generated for the 1-D model. These 3-D-model-based correction factors were then applied to the field data and an inversion was performed ignoring the boreholes. The resultant model displayed in Figure 4.8c and d is very similar to that presented in Figure 4.6a and b, with a correlation coefficient of 0.98 between the two models.

Of course, in practice, the true model is not known in advance, so using correction factors based on the final 3-D model is not feasible. Since correction factors based on a 1-D starting model are demonstrably insufficient, the only satisfactory approach to account for the borehole-fluid effect is to represent the boreholes in an appropriate unstructured mesh and explicitly include them in the inversion process.

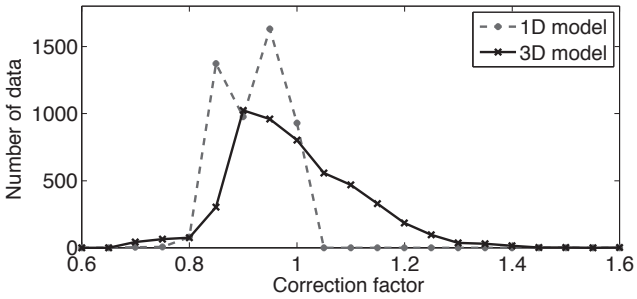

Figure 4.7. Frequency polygons of borehole-correction factors based on apparent-resistivity ratios computed for each electrode configuration with and without the boreholes. The two curves are for the layered (1-D) model of Table 4.1 and the actual 3-D inverted model in Figure 4.6c and d. The difference in the patterns is quite large.

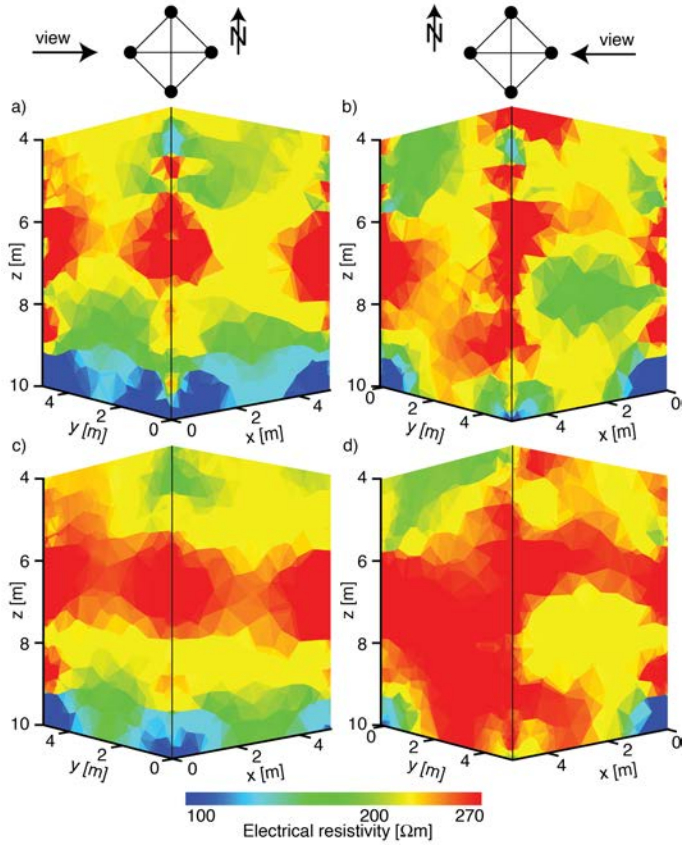

Figure 4.8. (a) and (b) 3-D inversion result using the program BERT with an unstructured mesh after first correcting the input data for the borehole effects according to the layered model of Table 4.1 and then ignoring the boreholes in the actual inversion. Note the high resistivity artifacts around the boreholes compared to Figure 4.6a and b. (c) and (d) As for (a) and (b), but first correcting the input data for the borehole effect according to the 3-D inversion result of Figure 4.6a and b. The result is quite similar to that of Figure 4.6a and b. Of course, one would not have the true model (i.e., Figure 4.6a and b) to make such corrections in practice, so the only purpose of doing it here is to emphasize the inadequacy of corrections based on the 1-D model (albeit with the approximately correct background resistivity). Note that the color bar is clipped at each end so that any resistivities lower than 100 Ωm remains blue and any resistivity higher than 270 Ωm remains red.

1.6 CONCLUSIONS

We have undertaken a systematic investigation of the influence of fluid-filled boreholes on the modeling and inversion of crosshole-ERT data. Our study is the first to include the boreholes and their fluid fill in the inversion process. This was achieved by representing the borehole by a dense network of elements in an unstructured mesh. The most important conclusions to emerge can be summarized as follows.

- The electrical resistivity structure of the ground, the resistivity contrast between the rock formation and borehole fluid, as well as survey design/geometrical factors (e.g., the borehole diameter, depth, hole spacing, electrode recording configuration) all play an important role in the borehole-fluid effect. This effect intensifies as the resistivity contrast $\rho_r : \rho_f$ and borehole diameter increase, and as the bipole spacing decreases. For AB-MN configurations, the apparent resistivities are underestimated whereas for AM-BN configurations they are overestimated.
- At our field study site, a very low resistivity contrast of 8 : 1 between the rock formation and the borehole fluid in the 11.4-cm-diameter boreholes produces artifacts that are much more significant than predicted by synthetic modeling; the effect appears to be severe even for the 5-cm-diameter boreholes used in complementary time-lapse ERT investigations at the site (results not presented here). Our results show that the effect is minor for forward modeling borehole diameters < 10 cm and a resistivity contrast of 10 : 1, but the effect greatly intensifies for inversions, such that significant artifacts can be produced in an inversion model; such error amplification effects are well known in seismic tomography.
- Correction factors based on simulations for a 1-D resistivity model with and without boreholes does not allow an inversion procedure that ignores the boreholes to recover the subsurface resistivity distribution.
- Trustworthy models of minor electrical resistivity variations based on ERT data acquired in fluid-filled boreholes can only be achieved by including the boreholes in the inversion. This is not really feasible with structured grids and necessitates an unstructured mesh approach. Time-lapse inversion utilizing ratios or differences of apparent resistivities or voltages is likely to be less influenced by the borehole effect and could be a partial remedy to the problem. However, this requires further investigation. In a strict theoretical sense, the sensitivity kernels

required in the inversion-parameter updates at each iteration to resolve subtle electrical resistivity variations should be based on an accurate model that incorporates the boreholes.

- Since the inclusion of particularly small boreholes increases the number of tetrahedral, this could increase the memory and run time of the inversion process considerably. In the case of a constant borehole fluid conductivity one could easily combine the inversion cells of each borehole to one unknown, which is possible with the code used.
- If unstructured-mesh numerical modeling and inversion capability is not available to practitioners, then our advice would be to use an alternative to fluid coupling of the electrodes in the boreholes. Examples would include electrodes mounted on the outside of a PVC pipe in an air-filled hole and held in firm contact with air-filled borehole walls.

REFERENCES

Acworth, R. I., and Dasey, G. R., 2003. Mapping of the hyporheic zone around a tidal creek using a combination of borehole logging, borehole electrical tomography and cross-creek electrical imaging, New South Wales, Australia, *Hydrogeology Journal*, **11**, 368-377.

Ajo-Franklin, J. B., Minsley, B. J., and Daley, T. M., 2007. Applying compactness constraints to differential traveltime tomography, *Geophysics*, **72**, R67-R75.

al Hagrey, S. A., and Müller, C., 2000. GPR study of pore water content and salinity in sand, *Geophysical Prospecting*, **48**, 63-85.

Allègre, V., Jouniaux, L., Lehmann, F., and Sailhac, P., 2010. Streaming potential dependence on water-content in Fontainebleau sand, *Geophysical Journal International*, **182**, 1248-1266.

Alumbaugh, D., Chang, P. Y., Paprocki, L., Brainard, J. R., Glass, R. J., and Rautman, C. A., 2002. Estimating moisture contents in the vadose zone using cross-borehole ground penetrating radar: A study of accuracy and repeatability, *Water Resources Research*, **38**, 1309.

Alumbaugh, D. L., and Newman, G. A., 2000. Image appraisal for 2-D and 3-D electromagnetic inversion, *Geophysics*, **65**, 1455-1467.

Annan, A. P., 2005. GPR Methods for Hydrogeological Studies, in *Hydrogeophysics*, edited by Y. Rubin and S. S. Hubbard, pp. 185-213, Springer Netherlands.

Archie, G. E., 1942. The electrical resistivity log as an aid in determining some reservoir characteristics, *Transactions of the American institute of Mining, Metallurgical and Petroleum Engineers*, **146**, 54-62.

Arora, T., Linde, N., Revil, A., and Castermant, J., 2007. Non-intrusive characterization of the redox potential of landfill leachate plumes from self-potential data, *Journal of Contaminant Hydrology*, **92**, 274-292.

Aubert, M., and Yéené Atangana, Q., 1996. Self-potential method in hydrogeological exploration of volcanic areas, *Ground Water*, **34**, 1010-1016.

Avseth, P., Mukerji, T., Jørstad, A., Mavko, G., and Veggeland, T., 2001. Seismic reservoir mapping from 3-D AVO in a North Sea turbidite system, *Geophysics*, **66**, 1157-1176.

BAFU, 2010. Hydrologischer Atlas der Schweiz, *Bundeamt für Umwelt, Bern, Switzerland*.

Barrash, W., and Clemo, T., 2002. Hierarchical geostatistics and multifacies systems: Boise Hydrogeophysical Research Site, Boise, Idaho, *Water Resources Research*, **38**, 1196.

Barrenetxea, G., Ingelrest, F., Schaefer, G., and Vetterli, M., 2008. The hitchhiker's guide to successful wireless sensor network deployments, *Sensys'08: Proceedings of the 6th Acm Conference on Embedded Networked Sensor Systems*, 43-56.

Battin, T. J., and Sengschmitt, D., 1999. Linking sediment biofilms, hydrodynamics, and river bed clogging: Evidence from a large river, *Microbial Ecology*, **37**, 185-196.

Baumann, M., Jordan, P., Hoehn, E., and Geisser, H., 2009. Ein neues Grundwassermodell für das Thurtal, *Mitteilungen der Thurgauischen Naturforschenden Gesellschaft*, **63**.

Bedrosian, P. A., Maercklin, N., Weckmann, U., Bartov, Y., Ryberg, T., and Ritter, O., 2007. Lithology-derived structure classification from the joint interpretation of magnetotelluric and seismic models, *Geophysical Journal International*, **170**, 737-748.

Bélanger, C., Giroux, B., Gloaguen, E., and Lefebvre, R., 2010. GPR, ERT and CPT data integration for high resolution aquifer modeling, *13th International Conference on GPR*, 1-6.

Belghoul, A., 2007. *Caractérisation petrophysique et hydrodynamique du socle cristallin*: PhD thesis, University of Montpellier.

Belina, F. A., Ernst, J. R., and Holliger, K., 2009. Inversion of crosshole seismic data in heterogeneous environments: Comparison of waveform and ray-based approaches, *Journal of Applied Geophysics*, **68**, 85-94.

Bencala, K. E., 1984. Interactions of solutes and streambed sediment 2. A dynamic analysis of coupled hydrologic and chemical processes that determine solute transport, *Water Resources Research*, **20**, 1804-1814.

Beres, M., Green, A., Huggenberger, P., and Horstmeyer, H., 1995. Mapping the architecture of glaciofluvial sediments with 3-dimensional georadar, *Geology*, **23**, 1087-1090.

Beres, M., Huggenberger, P., Green, A. G., and Horstmeyer, H., 1999. Using two- and three-dimensional georadar methods to characterize glaciofluvial architecture, *Sedimentary Geology*, **129**, 1-24.

Bernhardt, E. S., Palmer, M. A., Allan, J. D., Alexander, G., Barnas, K., et al., 2005. Ecology - Synthesizing US river restoration efforts, *Science*, **308**, 636-637.

Beutel, J., Dyer, M., Lim, R., Plessl, C., Wohrle, M., et al., 2007. Automated wireless sensor network testing, *INSS 07: Proceedings of the Fourth International Conference on Networked Sensing Systems*, 303-303.

Beven, K., and Binley, A., 1992. The future of distributed models - model calibration and uncertainty prediction, *Hydrological Processes*, **6**, 279-298.

Bing, Z., and Greenhalgh, S. A., 1998a. A damping method for the computation of the 2.5-D Green's function for arbitrary acoustic media, *Geophysical Journal International*, **133**, 111-120.

Bing, Z., and Greenhalgh, S. A., 1998b. Crosshole acoustic velocity imaging with full-waveform spectral data: 2.5-D numerical simulations, *Exploration Geophysics*, **29**, 680-684.

Bing, Z., and Greenhalgh, S. A., 2000. Cross-hole resistivity tomography using different electrode configurations, *Geophysical Prospecting*, **48**, 887-912.

Binley, A., Winship, P., Middleton, R., Pokar, M., and West, J., 2001. High-resolution characterization of vadose zone dynamics using cross-borehole radar, *Water Resources Research*, **37**, 2639-2652.

Binley, A., Winship, P., West, L. J., Pokar, M., and Middleton, R., 2002a. Seasonal variation of moisture content in unsaturated sandstone inferred from borehole radar and resistivity profiles, *Journal of Hydrology*, **267**, 160-172.

Binley, A., Cassiani, G., Middleton, R., and Winship, P., 2002b. Vadose zone flow model parameterisation using cross-borehole radar and resistivity imaging, *Journal of Hydrology*, **267**, 147-159.

Binley, A., Cassiani, G., and Deiana, R., 2010. Hydrogeophysics: Opportunities and challenges, *Bollettino di Geofisica Teorica ed Applicata*, **51**, 267-284.

Birchak, J. R., Gardner, C. G., Hipp, J. E., and Victor, J. M., 1974. High dielectric constant microwave probes for sensing soil moisture, *Proceedings of the IEEE*, **62**, 93-98.

Bleistein, N., 1986. 2-1/2 dimensional inplane wave-propagation, *Geophysical Prospecting*, **34**, 686-703.

Blome, M., Maurer, H. R., and Schmidt, K., 2009. Advances in three-dimensional geoelectric forward solver techniques, *Geophysical Journal International*, **176**, 740-752.

Blome, M., Maurer, H., and Greenhalgh, S., 2011. Geoelectric experimental design - Efficient acquisition and exploitation of complete pole-bipole data sets, *Geophysics*, **76**, F15-F26.

Boggs, J. M., and Adams, E. E., 1992. Field study of dispersion in a heterogeneous aquifer: 4. Investigation of adsorption and sampling bias, *Water Resources Research*, **28**, 3325-3336.

Boggs, J. M., Young, S. C., Beard, L. M., Gelhar, L. W., Rehfeldt, K. R., and Adams, E. E., 1992. Field-study of dispersion in a heterogeneous aquifer: 1. Overview and site description, *Water Resources Research*, **28**, 3281-3291.

Bohlen, T., 2002. Parallel 3-D viscoelastic finite difference seismic modelling, *Computers & Geosciences*, **28**, 887-899.

Bolève, A., Revil, A., Janod, F., Mattiuzzo, J. L., and Fry, J. J., 2009. Preferential fluid flow pathways in embankment dams imaged by self-potential tomography, *Near Surface Geophysics*, **7**, 447-462.

Bosma, T. N. P., Ballemans, E. M. W., Hoekstra, N. K., teWelscher, R. A. G., Smeenk, J. G. M. M., et al., 1996. Biotransformation of organics in soil columns and an infiltration area, *Ground Water*, **34**, 49-56.

Bouman, C. A., 1997. Cluster: An unsupervised algorithm for modeling Gaussian mixtures, http://www.ece.purdue.edu/~bouman.

Bourg, A. C. M., and Bertin, C., 1993. Biogeochemical processes during the infiltration of river water into an alluvial aquifer, *Environmental Science & Technology*, **27**, 661-666.

Bouwer, H., and Rice, R. C., 1976. Slug test for determining hydraulic conductivity of unconfined aquifers with completely or partially penetrating wells, *Water Resources Research*, **12**, 423-428.

Bowling, J. C., Rodriguez, A. B., Harry, D. L., and Zheng, C., 2005. Delineating alluvial aquifer heterogeneity using resistivity and GPR data, *Ground Water*, **43**, 890-903.

Bowling, J. C., Harry, D. L., Rodriguez, A. B., and Zheng, C., 2007. Integrated geophysical and geological investigation of a heterogeneous fluvial aquifer in Columbus Mississippi, *Journal of Applied Geophysics*, **62**, 58-73.

Bradford, J. H., Clement, W. P., and Barrash, W., 2009. Estimating porosity with ground-penetrating radar reflection tomography: A controlled 3-D experiment at the Boise Hydrogeophysical Research Site, *Water Resources Research*, **45**, W00D26.

Brookes, A., 1988. *Channelized rivers: Prospectives for environmental management*, John Wiley and Sons, Chichester, UK.

Brovelli, A., and Cassiani, G., 2010. A combination of the Hashin-Shtrikman bounds aimed at modelling electrical conductivity and permittivity of variably saturated porous media, *Geophysical Journal International*, **180**, 225-237.

Brunke, M., and Gonser, T., 1997. The ecological significance of exchange processes between rivers and groundwater, *Freshwater Biology*, **37**, 1-33.

Butler, A. P., Mathias, S. A., Gallagher, A. J., Peach, D. W., and Williams, A. T., 2009. Analysis of flow processes in fractured chalk under pumped and ambient conditions (UK), *Hydrogeology Journal*, **17**, 1849-1858.

Butler, J. J., 1998. *The design, performance and analysis of slug tests*, Lewis, Boca Raton.

Butler, J. J., Garnett, E. J., and Healey, J. M., 2003. Analysis of slug tests in formations of high hydraulic conductivity, *Ground Water*, **41**, 620-630.

BUWAL, 2004. Wegleitung Grundwasserschutz, *Bundesamt für Umwelt, Wald und Landschaft, Bern, Switzerland*.

Carcione, J. M., Ursin, B., and Nordskag, J. I., 2007. Cross-property relations between electrical conductivity and the seismic velocity of rocks, *Geophysics*, **72**, E193-E204.

Cardenas, M. B., Wilson, J. L., and Zlotnik, V. A., 2004. Impact of heterogeneity, bed forms, and stream curvature on subchannel hyporheic exchange, *Water Resources Research*, **40**, W08307.

Cardenas, M. B., and Markowski, M. S., 2011. Geoelectrical imaging of hyporheic exchange and mixing of river water and groundwater in a large regulated river, *Environmental Science & Technology*, **45**, 1407-1411.

Carsel, R. F., and Parrish, R. S., 1988. Developing joint probability-distributions of soil-water retention characteristics, *Water Resources Research*, **24**, 755-769.

Caruthers, R. M., and Smith, I. F., 1992. The use of ground electrical survey methods for siting water-supply boreholes in shallow crystalline basement terrains, in *Hydrogeology of Crystalline Basement Aquifers in Africa*, edited by E. P. Wright and W. G. Burgess, pp. 203-220, Geological Society Special Publication.

Cassiani, G., Bruno, V., Villa, A., Fusi, N., and Binley, A. M., 2006. A saline trace test monitored via time-lapse surface electrical resistivity tomography, *Journal of Applied Geophysics*, **59**, 244-259.

Chambers, J. E., Wilkinson, P. B., Weller, A. L., Meldrum, P. I., Gilvy, R. D., and Caunt, S., 2007. Mineshaft imaging using surface and crosshole 3D electrical resistivity tomography: A case history from the East Pennine Coalfield, UK, *Journal of Applied Geophysics*, **62**, 324-337.

Chen, J. S., Hubbard, S., Rubin, Y., Murray, C., Roden, E., and Majer, E., 2004. Geochemical characterization using geophysical data and Markov Chain Monte Carlo methods: A case study at the South Oyster bacterial transport site in Virginia, *Water Resources Research*, **40**, W12412.

Cirpka, O. A., Fienen, M. N., Hofer, M., Hoehn, E., Tessarini, A., et al., 2007. Analyzing bank filtration by deconvoluting time series of electric conductivity, *Ground Water*, **45**, 318-328.

Claerbout, J. F., and Muir, F., 1973. Robust modeling with erratic data, *Geophysics*, **38**, 826-844.

Constantz, J., Cox, M. H., and Su, G. W., 2003. Comparison of heat and bromide as ground water tracers near streams, *Ground Water*, **41**, 647-656.

Constantz, J., 2008. Heat as a tracer to determine streambed water exchanges, *Water Resources Research*, **44**, W00D10.

Coscia, I., Marescot, L., Maurer, H., Greenhalgh, S., and Linde, N., 2008. Experimental design for crosshole electrical resistivity tomography data sets, *14th Annual European Meeting of Environmental and Engineering Geophysics, EAGE.*

Coscia, I., Greenhalgh, S., Linde, N., Green, A., Günther, T., et al., 2010. A multi-borehole 3-D ERT monitoring system for aquifer characterization using river flood events as a natural tracer, *16th Annual European Meeting of Environmental and Engineering Geophysics, EAGE.*

Coscia, I., Greenhalgh, S. A., Linde, N., Doetsch, J., Marescot, L., et al., 2011a. 3D crosshole ERT for aquifer characterization and monitoring of infiltrating river water, *Geophysics*, **76**, G49-G59.

Coscia, I., Linde, N., Greenhalgh, S., Günther, T., and Green, A., 2011b. A deconvolution approach to correct time-lapse 3D ERT data and improve imaging of natural aquifer dynamics, *Water Resources Research*, under review.

Crook, N., Binley, A., Knight, R., Robinson, D. A., Zarnetske, J., and Haggerty, R., 2008. Electrical resistivity imaging of the architecture of substream sediments, *Water Resources Research*, **44**, W00D13.

Daily, W., and Owen, E., 1991. Cross-borehole resistivity tomography, *Geophysics*, **56**, 1228-1235.

Daily, W., Ramirez, A., Labrecque, D., and Nitao, J., 1992. Electrical resistivity tomography of vadose water movement, *Water Resources Research*, **28**, 1429-1442.

Daily, W., and Ramirez, A., 1995. Electrical-resistance tomography during in-situ trichloroethylene remediation at the savanna river site, *Journal of Applied Geophysics*, **33**, 239-249.

Daily, W., Ramirez, A., Binley, A., and LaBrecque, D., 2005. Electrical resistance tomography — theory and practice, in *Near surface geophysics*, edited by D. K. Butler, pp. 525-550, SEG.

Daniels, J. J., Allred, B., Binley, A., Labrecque, D., and Alumbaugh, D., 2005. Hydrogeophysical case studies in the vadose zone, in *Hydrogeophysics*, edited by Y. Rubin and S. S. Hubbard, pp. 413-440, Springer.

Darling, T., 2005. *Well logging and formation evaluation*, Elsevier.

Darnet, M., and Marquis, G., 2004. Modelling streaming potential (SP) signals induced by water movement in the vadose zone, *Journal of Hydrology*, **285**, 114-124.

Day-Lewis, F. D., Lane, J. W., Jr., Harris, J. M., and Gorelick, S. M., 2003. Time-lapse imaging of saline-tracer transport in fractured rock using difference-attenuation radar tomography, *Water Resources Research*, **39**, 1290.

Day-Lewis, F. D., and Lane, J. W., 2004. Assessing the resolution-dependent utility of tomograms for geostatistics, *Geophysical Research Letters*, **31**, L07503.

Day-Lewis, F. D., Singha, K., and Binley, A. M., 2005. Applying petrophysical models to radar travel time and electrical resistivity tomograms: Resolution-dependent limitations, *Journal of Geophysical Research-Solid Earth*, **110**, B08206.

Day-Lewis, F. D., Lane, J. W., and Gorelick, S. M., 2006. Combined interpretation of radar, hydraulic, and tracer data from a fractured-rock aquifer near Mirror Lake, New Hampshire, USA, *Hydrogeology Journal*, **14**, 1-14.

Day-Lewis, F. D., Chen, Y., and Singha, K., 2007. Moment inference from tomograms, *Geophysical Research Letters*, **34**, L22404.

de Franco, R., Biella, G., Tosi, L., Teatini, P., Lozej, A., et al., 2009. Monitoring the saltwater intrusion by time lapse electrical resistivity tomography: The Chioggia test site (Venice Lagoon, Italy), *Journal of Applied Geophysics*, **69**, 117-130.

Deiana, R., Cassiani, G., Kemna, A., Villa, A., Bruno, V., and Bagliani, A., 2007. An experiment of non-invasive characterization of the vadose zone via water injection and cross-hole time-lapse geophysical monitoring, *Near Surface Geophysics*, **5**, 183-194.

Dempster, A. P., Laird, N. M., and Rubin, D. B., 1977. Maximum likelihood from incomplete data via the EM algorithm, *Journal of the Royal Statistical Society, Series B (Methodological)*, **39**, 1-38.

Deutsch, C. V., and Journel, A. G., 1998. *GSLIB: Geostatistical software library and user's guide*, 2. edition ed., Oxford Univ. Press, New York, 2. edition.

Diem, S., Vogt, T., and Hoehn, E., 2010. Räumliche Charakterisierung der hydraulischen Leitfähigkeit in alluvialen Schotter-Grundwasserleitern: Ein Methodenvergleich, *Grundwasser*, **15**, 241-251.

Dietrich, C. R., and Newsam, G. N., 1997. Fast and exact simulation of stationary Gaussian processes through circulant embedding of the covariance matrix, *Siam Journal on Scientific Computing*, **18**, 1088-1107.

Dogan, M., Van Dam, R. L., Bohling, G. C., Butler, J. J., Jr., and Hyndman, D. W., 2011. Hydrostratigraphic analysis of the MADE site with full-resolution GPR and direct-push hydraulic profiling, *Geophysical Research Letters*, **38**, L06405.

Dorn, C., Linde, N., Le Borgne, T., Bour, O., and Baron, L., 2011. Single-hole GPR reflection imaging of solute transport in a granitic aquifer, *Geophysical Research Letters*, **38**, L08401.

Doussan, C., Jouniaux, L., and Thony, J. L., 2002. Variations of self-potential and unsaturated water flow with time in sandy loam and clay loam soils, *Journal of Hydrology*, **267**, 173-185.

EC, 2000. Directive 2000/60/EC of the European Parliament and of the council establishing a framework for community action in the field of water policy, *Official Journal of the European Community*, **L327**, 1-72.

Eckert, P., Lamberts, R., and Wagner, C., 2008. The impact of climate change on drinking water supply by riverbank filtration, *Water Science Technology*, **8**, 319-324.

Edmaier, K., Burlando, P., and Perona, P., 2011. Mechanisms of vegetation uprooting by flow in alluvial non-cohesive sediment, *Hydrology and Earth Systems Science Discussion*, **8**, 1365-1398.

Eisenberg, D., and Kauzmann, W., 1969. *The structure and properties of water*, Oxford University Press.

Ellis, R. G., and Oldenburg, D. W., 1994. Applied geophysical inversion, *Geophysical Journal International*, **116**, 5-11.

Eppstein, M. J., and Dougherty, D. E., 1998. Optimal 3-D traveltime tomography, *Geophysics*, **63**, 1053-1061.

Ernst, J. R., Maurer, H., Green, A. G., and Holliger, K., 2007a. Full-waveform inversion of crosshole radar data based on 2-D finite-difference time-domain solutions of Maxwell's equations, *Ieee Transactions on Geoscience and Remote Sensing*, **45**, 2807-2828.

Ernst, J. R., Green, A. G., Maurer, H., and Holliger, K., 2007b. Application of a new 2D time-domain full-waveform inversion scheme to crosshole radar data, *Geophysics*, **72**, J53-J64.

Ernst, J. R., 2007. *2-D finite-difference time-domain full-waveform inversion of crosshole georadar data*: PhD thesis, ETH Zurich.

Farquharson, C. G., 2008. Constructing piecewise-constant models in multidimensional minimum-structure inversions, *Geophysics*, **73**, K1-K9.

Favetto, A., Pomposiello, C., Booker, J., and Rossello, E. A., 2007. Magnetotelluric inversion constrained by seismic data in the Tucuman basin (Andean foothills, 27 degrees S, NW argentina), *Journal of Geophysical Research - Solid Earth*, **112**, B09104.

Fine, R. A., and Millero, F. J., 1973. Compressibility of water as a function of temperature and pressure, *Journal of Chemical Physics*, **59**, 5529-5536.

Fleckenstein, J. H., Niswonger, R. G., and Fogg, G. E., 2006. River-aquifer interactions, geologic heterogeneity, and low-flow management, *Ground Water*, **44**, 837-852.

Fournier, C., 1989. Spontaneous potentials and resistivity surveys applied to hydrogeology in a volcanic area - case-history of the Chaine-Des-Puys (Puy-De-Dome, France), *Geophysical Prospecting*, **37**, 647-668.

Fregoso, E., and Gallardo, L. A., 2009. Cross-gradients joint 3D inversion with applications to gravity and magnetic data, *Geophysics*, **74**, L31-L42.

French, H., and Binley, A., 2004. Snowmelt infiltration: Monitoring temporal and spatial variability using time-lapse electrical resistivity, *Journal of Hydrology*, **297**, 174-186.

Friedel, S., 2003. Resolution, stability and efficiency of resistivity tomography estimated from a generalized inverse approach, *Geophysical Journal International*, **153**, 305-316.

Friedel, S., Byrdina, S., Jacobs, F., and Zimmer, M., 2004. Self-potential and ground temperature at Merapi volcano prior to its crisis in the rainy season of 2000-2001, *Journal of Volcanology and Geothermal Research*, **134**, 149-168.

Füchtenbauer, H., 1988. *Sedimente und Sedimentgesteine: Sandsteine*, 4 ed., Schweizerbart, Stuttgart.

Gallardo, L. A., and Meju, M. A., 2003. Characterization of heterogeneous near-surface materials by joint 2D inversion of dc resistivity and seismic data, *Geophysical Research Letters*, **30**, 1658.

Gallardo, L. A., and Meju, M. A., 2004. Joint two-dimensional DC resistivity and seismic travel time inversion with cross-gradients constraints, *Journal of Geophysical Research - Solid Earth*, **109**, B03311.

Gallardo, L. A., Meju, M. A., and Pérez-Flores, M. A., 2005. A quadratic programming approach for joint image reconstruction: Mathematical and geophysical examples, *Inverse Problems*, **21**, 435-452.

Gallardo, L. A., 2007. Multiple cross-gradient joint inversion for geospectral imaging, *Geophysical Research Letters*, **34**, L19301.

Gallardo, L. A., and Meju, M. A., 2007. Joint two-dimensional cross-gradient imaging of magnetotelluric and seismic traveltime data for structural and lithological classification, *Geophysical Journal International*, **169**, 1261-1272.

Gallardo, L. A., and Meju, M. A., 2011. Structure-Coupled Multiphysics Imaging in Geophysical Sciences, *Reviews of Geophysics*, **49**, RG1003.

Garambois, S., Senechal, P., and Perroud, H., 2002. On the use of combined geophysical methods to assess water content and water conductivity of near-surface formations, *Journal of Hydrology*, **259**, 32-48.

Gasperikova, E., Zhang, Y., and Hubbard, S., 2008. Using self potential and multiphase flow modeling to optimize groundwater pumping*, EOS Transactions AGU, 89(53)*.

Giannopoulos, A., 2005. Modelling ground penetrating radar by GprMax, *Construction and Building Materials*, **19**, 755-762.

Gibert, D., and Pessel, M., 2001. Identification of sources of potential fields with the continuous wavelet transform: Application to self-potential profiles, *Geophysical Research Letters*, **28**, 1863-1866.

Golub, G. H., and van Loan, C. F., 1996. *Matrix computations*, Johns Hopkins University Press.

Gooseff, M. N., Anderson, J. K., Wondzell, S. M., LaNier, J., and Haggerty, R., 2005. A modelling study of hyporheic exchange pattern and the sequence, size, and spacing of stream bedforms in mountain stream networks, Oregon, USA, *Hydrological Processes*, **19**, 2915-2929.

Grasmueck, M., 1996. 3-D ground-penetrating radar applied to fracture imaging in gneiss, *Geophysics*, **61**, 1050-1064.

Grinsted, A., Moore, J. C., and Jevrejeva, S., 2004. Application of the cross wavelet transform and wavelet coherence to geophysical time series, *Nonlinear Processes in Geophysics*, **11**, 561-566.

GschG, 1991. Gewaesserschutzgesetz,, *Bundesgesetz über den Schutz der Gewässer, Schweiz*, **814.20**, 30.

GSchV, 1998. Gewaesserschutzverordnung, *Bundesgesetz über den Schutz der Gewässer, Schweiz*, **814.201**, 60.

Günther, T., 2004. *Inversion methods and resolution analysis for the 2D/3D reconstruction of resistivity structures from DC measurements*, Ph.D. thesis thesis: TU Bergakademie Freiberg.

Günther, T., and Rücker, C., 2006. A general approach for introducing information into inversion and examples from dc resistivity inversion, in *14th Annual European Meeting of Environmental and Engineering Geophysics*, edited, p. P039, EAGE.

Günther, T., Rücker, C., and Spitzer, K., 2006. Three-dimensional modelling and inversion of dc resistivity data incorporating topography - II. Inversion, *Geophysical Journal International*, **166**, 506-517.

Günther, T., and Rücker, C., 2009. Advanced inversion strategies using a new geophysical inversion and modelling library, *15th Annual European Meeting of Environmental and Engineering Geophysics, EAGE.*

Haber, E., and Oldenburg, D., 1997. Joint inversion: A structural approach, *Inverse Problems*, **13**, 63-77.

Harbaugh, A. W., 2005. MODFLOW-2005, The U.S. Geological Survey modular ground-water model—the ground-water flow process, in *Book 6. Modeling techniques*, Ch. 16.

Harvey, J. W., and Bencala, K. E., 1993. The effect of streambed topography on surface-subsurface water exchange in mountain catchments, *Water Resources Research*, **29**, 89-98.

Hashin, Z., and Shtrikman, S., 1962. A variational approach to theory of effective magnetic permeability of multiphase materials, *Journal of Applied Physics*, **33**, 3125-&.

Hashin, Z., and Shtrikman, S., 1963. A variational approach to the theory of the elastic behaviour of multiphase materials, *Journal of the Mechanics and Physics of Solids*, **11**, 127-140.

Hatch, C. E., Fisher, A. T., Revenaugh, J. S., Constantz, J., and Ruehl, C., 2006. Quantifying surface water-groundwater interactions using time series analysis of streambed thermal records: Method development, *Water Resources Research*, **42**, W10410.

Hauck, C., 2002. Frozen ground monitoring using DC resistivity tomography, *Geophysical Research Letters*, **29**, 2016.

Hayley, K., Bentley, L. R., and Gharibi, M., 2009. Time-lapse electrical resistivity monitoring of salt-affected soil and groundwater, *Water Resources Research*, **45**.

Heinz, J., Kleineidam, S., Teutsch, G., and Aigner, T., 2003. Heterogeneity patterns of quaternary glaciofluvial gravel bodies (SW-Germany): Application to hydrogeology, *Sedimentary Geology*, **158**, 1-23.

Henderson, R. D., Day-Lewis, F. D., and Harvey, C. F., 2009. Investigation of aquifer-estuary interaction using wavelet analysis of fiber-optic temperature data, *Geophysical Research Letters*, **36**, L06403.

Hiscock, K. M., and Grischek, T., 2002. Attenuation of groundwater pollution by bank filtration, *Journal of Hydrology*, **266**, 139-144.

Hoehn, E., and Cirpka, O. A., 2006. Assessing residence times of hyporheic ground water in two alluvial flood plains of the Southern Alps using water temperature and tracers, *Hydrology and Earth System Sciences*, **10**, 553-563.

Hoehn, E., and Scholtis, A., 2011. Exchange between a river and groundwater, assessed with hydrochemical data, *Hydrology and Earth System Sciences*, **15**, 983-988.

Hollender, F., Tillard, S., and Corin, L., 1999. Multifold borehole radar acquisition and processing, *Geophysical Prospecting*, **47**, 1077-1090.

Holliger, K., Musil, M., and Maurer, H. R., 2001. Ray-based amplitude tomography for crosshole georadar data: A numerical assessment, *Journal of Applied Geophysics*, **47**, 285-298.

Hu, W. Y., Abubakar, A., and Habashy, T. M., 2009. Joint electromagnetic and seismic inversion using structural constraints, *Geophysics*, **74**, R99-R109.

Hubbard, S., and Linde, N., 2011. Hydrogeophysics, in *Treatise on water*, edited by P. Wilderer, Ch. 43, Elsevier.

Hubbard, S. S., Rubin, Y., and Majer, E., 1999. Spatial correlation structure estimation using geophysical and hydrogeological data, *Water Resources Research*, **35**, 1809-1825.

Hubbard, S. S., Chen, J. S., Peterson, J., Majer, E. L., Williams, K. H., et al., 2001. Hydrogeological characterization of the South Oyster Bacterial Transport Site using geophysical data, *Water Resources Research*, **37**, 2431-2456.

Huggenberger, P., 1993. Radar facies: Recognition of facies patterns and heterogeneities within Pleistocene Rhine gravels, NE Switzerland, *Geological Society, London, Special Publications*, **75**, 163-176.

Huggenberger, P., Hoehn, E., Beschta, R., and Woessner, W., 1998. Abiotic aspects of channels and floodplains in riparian ecology, *Freshwater Biology*, **40**, 407-425.

Hyndman, D. W., and Gorelick, S. M., 1996. Estimating lithologic and transport properties in three dimensions using seismic and tracer data: The Kesterson aquifer, *Water Resources Research*, **32**, 2659-2670.

Hyndman, D. W., and Harris, J. M., 1996. Traveltime inversion for the geometry of aquifer lithologies, *Geophysics*, **61**, 1728-1737.

Jackson, M. D., 2010. Multiphase electrokinetic coupling: Insights into the impact of fluid and charge distribution at the pore scale from a bundle of capillary tubes model, *Journal of Geophysical Research-Solid Earth*, **115**, B07206.

Jacobs, L. A., Vongunten, H. R., Keil, R., and Kuslys, M., 1988. Geochemical changes along a river-groundwater infiltration flow path - Glattfelden, Switzerland, *Geochimica Et Cosmochimica Acta*, **52**, 2693-2706.

Jakubowicz, H., 1990. A simple efficient method of dip-moveout correction, *Geophysical Prospecting*, **38**, 221-245.

Jardani, A., Revil, A., Boleve, A., Crespy, A., Dupont, J. P., et al., 2007. Tomography of the Darcy velocity from self-potential measurements, *Geophysical Research Letters*, **34**, L24403.

Jayawickreme, D. H., Van Dam, R. L., and Hyndman, D. W., 2008. Subsurface imaging of vegetation, climate, and root-zone moisture interactions, *Geophysical Research Letters*, **35**, L18404.

Jegen, M. D., Hobbs, R. W., Tarits, P., and Chave, A., 2009. Joint inversion of marine magnetotelluric and gravity data incorporating seismic constraints: Preliminary results of sub-basalt imaging off the Faroe Shelf, *Earth and Planetary Science Letters*, **282**, 47-55.

Jougnot, D., Ghorbani, A., Revil, A., Leroy, P., and Cosenza, P., 2010. Spectral induced polarization of partially saturated clay-rocks: A mechanistic approach, *Geophysical Journal International*, **180**, 210-224.

Jung, H. K., Min, D. J., Lee, H. S., Oh, S., and Chung, H., 2009. Negative apparent resistivity in dipole-dipole electrical surveys, *Exploration Geophysics*, **40**, 33-40.

Kalbus, E., Reinstorf, F., and Schirmer, M., 2006. Measuring methods for groundwater - surface water interactions: A review, *Hydrology and Earth System Sciences*, **10**, 873-887.

Kalbus, E., Schmidt, C., Molson, J. W., Reinstorf, F., and Schirmer, M., 2009. Influence of aquifer and streambed heterogeneity on the distribution of groundwater discharge, *Hydrology and Earth System Sciences*, **13**, 69-77.

Keery, J., Binley, A., Crook, N., and Smith, J. W. N., 2007. Temporal and spatial variability of groundwater-surface water fluxes: Development and application of an analytical method using temperature time series, *Journal of Hydrology*, **336**, 1-16.

Keller, G. V., and Frischknecht, F., 1966. *Electrical methods in geophysical prospecting*, Pergamon.

Kemna, A., Kulessa, B., and Vereecken, H., 2002. Imaging and characterisation of subsurface solute transport using electrical resistivity tomography (ERT) and equivalent transport models, *Journal of Hydrology*, **267**, 125-146.

Khalil, A. A., Stewart, R. R., and Henley, D. C., 1993. Full-wave-form processing and interpretation of kilohertz cross-well seismic data, *Geophysics*, **58**, 1248-1256.

Kipfer, R., Aeschbach-Hertig, W., Peeters, F., and Stute, M., 2002. Noble gases in lakes and ground waters, *Noble Gases in Geochemistry and Cosmochemistry*, **47**, 615-700.

Klotzsche, A., van der Kruk, J., Meles, G. A., Doetsch, J., Maurer, H., and Linde, N., 2010. Full-waveform inversion of cross-hole ground-penetrating radar data to characterize a gravel aquifer close to the Thur River, Switzerland, *Near Surface Geophysics*, **8**, 635-649.

Knight, R. J., and Nur, A., 1987. The dielectric-constant of sandstones, 60 Khz to 4 Mhz, *Geophysics*, **52**, 644-654.

Koch, K., Wenninger, J., Uhlenbrook, S., and Bonell, M., 2009. Joint interpretation of hydrological and geophysical data: Electrical resistivity tomography results from a process hydrological research site in the Black Forest Mountains, Germany, *Hydrological Processes*, **23**, 1501-1513.

Kondolf, G. M., 1998. Lessons learned from river restoration projects in California, *Aquatic Conservation-Marine and Freshwater Ecosystems*, **8**, 39-52.

Kosinski, W. K., and Kelly, W. E., 1981. Geoelectric soundings for predicting aquifer properties, *Ground Water*, **19**, 163-171.

Kowalsky, M. B., Finsterle, S., Peterson, J., Hubbard, S., Rubin, Y., et al., 2005. Estimation of field-scale soil hydraulic and dielectric parameters through joint inversion of GPR and hydrological data, *Water Resources Research*, **41**, W11425.

Krautblatter, M., Verleysdonk, S., Flores-Orozco, A., and Kemna, A., 2010. Temperature-calibrated imaging of seasonal changes in permafrost rock walls by quantitative electrical resistivity

tomography (Zugspitze, German/Austrian Alps), *Journal of Geophysical Research-Earth Surface*, **115**, F02003.

Kruse, S., Grasmueck, M., Weiss, M., and Viggiano, D., 2006. Sinkhole structure imaging in covered Karst terrain, *Geophysical Research Letters*, **33**, L16405.

Kumar, P., and Foufoula-Georgiou, E., 1997. Wavelet analysis for geophysical applications, *Reviews of Geophysics*, **35**, 385-412.

Kuras, O., Pritchard, J. D., Meldrum, P. I., Chambers, J. E., Wilkinson, P. B., et al., 2009. Monitoring hydraulic processes with automated time-lapse electrical resistivity tomography (ALERT), *Comptes Rendus Geoscience*, **341**, 868-885.

Kuroda, S., Takeuchi, M., and Kim, H. J., 2007. Full-waveform inversion algorithm for interpreting crosshole radar data: A theoretical approach, *Geosciences Journal*, **11**, 211-217.

LaBrecque, D. J., Ramirez, A. L., Daily, W. D., Binley, A. M., and Schima, S. A., 1996a. ERT monitoring on environmental remediation processes, *Measurement Science & Technology*, **7**, 375-383.

LaBrecque, D. J., Miletto, M., Daily, W., Ramirez, A., and Owen, E., 1996b. The effects of noise on Occam's inversion of resistivity tomography data, *Geophysics*, **61**, 538-548.

LaBrecque, D. J., and Yang, X., 2001. Difference inversion of ERT data: A fast inversion method for 3-D in situ monitoring, *Journal of Environmental and Engineering Geophysics*, **6**, 83-89.

Lacey, G., 1930. Stable channel in alluvium, *Proceedings of the Institution of Civil Engineers*, **229**, 259-292.

Lane, J. W., Day-Lewis, F. D., and Casey, C. C., 2006. Geophysical monitoring of a field-scale biostimulation pilot project, *Ground Water*, **44**, 430-443.

Langevin, C. D., Thorne, D. T., Jr., Dausman, A. M., Sukip, M. C., and Guo, W., 2008. SEAWAT version 4: A computer program for simulation of multi-species solute and heat transport, in *USGS Techniques and Methods Book 6*, Ch. A22.

Langevin, C. D., 2009. SEAWAT: A computer program for simulation of variable-density groundwater flow and multi-species solute and heat transport, *U.S. Geological Survey*, Fact Sheet 2009-3047.

Lanz, E., Boerner, D. E., Maurer, H., and Green, A., 1998. Landfill delineation and characterization using electrical, electromagnetic and magnetic methods, *Journal of Environmental and Engineering Geophysics*, **3**, 185-196.

Lazaratos, S. K., Harris, J. M., Rector, J. W., and Vanschaack, M., 1995. High-resolution crosswell imaging of a west texas carbonate reservoir 4. Reflection imaging, *Geophysics*, **60**, 702-711.

Le Borgne, T., Bour, O., Paillet, F. L., and Caudal, J. P., 2006. Assessment of preferential flow path connectivity, and hydraulic properties at single-borehole and cross-borehole scales in a fractured aquifer, *Journal of Hydrology*, **328**, 347-359.

Le Borgne, T., Bour, O., Riley, M. S., Gouze, P., Pezard, P. A., et al., 2007. Comparison of alternative methodologies for identifying and characterizing preferential flow paths in heterogeneous aquifers, *Journal of Hydrology*, **345**, 134-148.

Leonard, B. P., 1991. The ULTIMATE conservative difference scheme applied to unsteady one-dimensional advection, *Computer Methods in Applied Mechanics and Engineering*, **88**, 17-74.

Lesmes, D. P., and Friedman, S. P., 2005. Relationships between the electrical and hydrogeological properties of rocks and soils, in *Hydrogeophysics*, edited by Y. Rubin and S. S. Hubbard, pp. 87-128, Springer.

Li, S. H., Unsworth, M. J., Booker, J. R., Wei, W. B., Tan, H. D., and Jones, A. G., 2003. Partial melt or aqueous fluid in the mid-crust of Southern Tibet? Constraints from INDEPTH magnetotelluric data, *Geophysical Journal International*, **153**, 289-304.

Linde, N., Binley, A., Tryggvason, A., Pedersen, L. B., and Revil, A., 2006a. Improved hydrogeophysical characterization using joint inversion of cross-hole electrical resistance and ground-penetrating radar traveltime data, *Water Resources Research*, **42**, W12404.

Linde, N., Finsterle, S., and Hubbard, S., 2006b. Inversion of tracer test data using tomographic constraints, *Water Resources Research*, **42**, W04410.

Linde, N., Jougnot, D., Revil, A., Matthäi, S. K., Arora, T., et al., 2007a. Streaming current generation in two-phase flow conditions, *Geophysical Research Letters*, **34**, L03306.

Linde, N., and Revil, A., 2007. Inverting self-potential data for redox potentials of contaminant plumes, *Geophysical Research Letters*, **34**, L14302.

Linde, N., Revil, A., Bolève, A., Dagès, C., Castermant, J., et al., 2007b. Estimation of the water table throughout a catchment using self-potential and piezometric data in a Bayesian framework, *Journal of Hydrology*, **334**, 88-98.

Linde, N., Tryggvason, A., Peterson, J. E., and Hubbard, S. S., 2008. Joint inversion of crosshole radar and seismic traveltimes acquired at the South Oyster Bacterial Transport Site, *Geophysics*, **73**, G29-G37.

Linde, N., and Doetsch, J. A., 2010. Joint inversion of crosshole GPR and seismic traveltime data, in *Advances in near-surface seismology and ground-penetrating radar*, edited by R. D. Miller, J. H. Bradford and K. Holliger, Ch. 1, pp. 1-18, Society of Exploration Geophysicists.

Linde, N., Doetsch, J., Jougnot, D., Genoni, O., Dürst, Y., et al., 2011. Self-potential investigations of a gravel bar in a restored river corridor, *Hydrology and Earth System Sciences*, **15**, 729-742.

Lines, L. R., Schultz, A. K., and Treitel, S., 1988. Cooperative inversion of geophysical data, *Geophysics*, **53**, 8-20.

Loke, M. H., and Barker, R. D., 1996. Practical techniques for 3D resistivity surveys and data inversion, *Geophysical Prospecting*, **44**, 499-523.

Long, J. C. S., Aydin, A., Brown, S. R., Einstein, H. H., Hestir, K., et al., 1996. *Rock fracture and fluid flow: Contemporary understanding and applications*, National Academy Press, Washington, DC.

Looms, M. C., Jensen, K. H., Binley, A., and Nielsen, L., 2008. Monitoring unsaturated flow and transport using cross-borehole geophysical methods, *Vadose Zone Journal*, **7**, 227.

Lowry, T., Allen, M. B., and Shive, P. N., 1989. Singularity removal: A refinement of resistivity modeling techniques, *Geophysics*, **54**, 766-774.

Lunt, I. A., Bridge, J. S., and Tye, R. S., 2004. A quantitative three-dimensional depositional model of gravelly braided rivers, *Sedimentology*, **51**, 1155-1155.

Maineult, A., Bernabe, Y., and Ackerer, P., 2004. Electrical response of flow, diffusion, and advection in a laboratory sand box, *Vadose Zone Journal*, **3**, 1180-1192.

Maineult, A., Bernabe, Y., and Ackerer, P., 2005. Detection of advected concentration and pH fronts from self-potential measurements, *Journal of Geophysical Research-Solid Earth*, **110**, B11205.

Maineult, A., Strobach, E., and Renner, J., 2008. Self-potential signals induced by periodic pumping tests, *Journal of Geophysical Research-Solid Earth*, **113**, B01203.

Mair, J. A., and Green, A. G., 1981. High-resolution seismic-reflection profiles reveal fracture-zones within a homogeneous granite batholith, *Nature*, **294**, 439-442.

Maraun, D., and Kurths, J., 2004. Cross wavelet analysis: Significance testing and pitfalls, *Nonlinear Processes in Geophysics*, **11**, 505-514.

Marescot, L., Rigobert, S., P. Lopes, S., Lagabrielle, R., and Chapellier, D., 2006. A general approach for DC apparent resistivity evaluation on arbitrarily shaped 3D structures, *Journal of Applied Geophysics*, **60**, 55-67.

Maurer, H., Holliger, K., and Boerner, D. E., 1998. Stochastic regularization: Smoothness or similarity?, *Geophysical Research Letters*, **25**, 2889-2892.

Maurer, H., and Musil, M., 2004. Effects and removal of systematic errors in crosshole georadar attenuation tomography, *Journal of Applied Geophysics*, **55**, 261-270.

Maurer, H., and Friedel, S., 2006. Outer-space sensitivities in geoelectrical tomography, *Geophysics*, **71**, G93-G96.

Maurer, H., Friedel, S., and Jaeggi, D., 2009. Characterization of a coastal aquifer using seismic and geoelectric borehole methods, *Near Surface Geophysics*, **7**, 353-366.

Mazac, O., Kelly, W. E., and Landa, I., 1987. Surface geoelectrics for groundwater pollution and protection studies, *Journal of Hydrology*, **93**, 277-294.

McClymont, A. F., Green, A. G., Streich, R., Horstmeyer, H., Tronicke, J., et al., 2008. Visualization of active faults using geometric attributes of 3D GPR data: An example from the Alpine Fault Zone, New Zealand, *Geophysics*, **73**, B11-B23.

McElwee, C. D., and Zenner, M. A., 1998. A nonlinear model for analysis of slug-test data, *Water Resources Research*, **34**, 55-66.

Meles, G. A., Van der Kruk, J., Greenhalgh, S. A., Ernst, J. R., Maurer, H., and Green, A. G., 2010. A new vector waveform inversion algorithm for simultaneous updating of conductivity and permittivity parameters from combination crosshole/borehole-to-surface GPR data, *Ieee Transactions on Geoscience and Remote Sensing*, **48**, 3391-3407.

Merkli, B., 1975. *Untersuchungen über Mechanismen und Kinetik der Elimination von Bakterien und Viren im Grundwasser*: ETH Zurich.

Miall, A. D., 1995. Description and interpretation of fluvial deposits - A critical perspective, *Sedimentology*, **42**, 379-384.

Michel, S., Salehi, A., Luo, L., Dawes, N., Aberer, K., et al., 2009. Environmental monitoring 2.0, *Icde: 2009 Ieee 25th International Conference on Data Engineering, Vols. 1-3*, 1507-1510.

Michot, D., Benderitter, Y., Dorigny, A., Nicoullaud, B., King, D., and Tabbagh, A., 2003. Spatial and temporal monitoring of soil water content with an irrigated corn crop cover using surface electrical resistivity tomography, *Water Resources Research*, **39**, 1138.

Miller, C. R., Routh, P. S., Brosten, T. R., and McNamara, J. P., 2008. Application of time-lapse ERT imaging to watershed characterization, *Geophysics*, **73**, G7-G17.

Minsley, B. J., 2007. *Modeling and inversion of self-potential data*: PhD thesis, Massachusetts Institute of Technology.

Minsley, B. J., Sogade, J., and Morgan, F. D., 2007. Three-dimensional source inversion of self-potential data, *Journal of Geophysical Research*, **112**.

Mitchell, T. M., 1997. *Machine learning*, McGraw-Hill, New York.

Monego, M., Cassiani, G., Deiana, R., Putti, M., Passadore, G., and Altissimo, L., 2010. A tracer test in a shallow heterogeneous aquifer monitored via time-lapse surface electrical resistivity tomography, *Geophysics*, **75**, WA61-WA73.

Monteiro Santos, F. A., Sultan, S. A., Represas, P., and El Sorady, A. L., 2006. Joint inversion of gravity and geoelectrical data for groundwater and structural investigation: Application to the northwestern part of Sinai, Egypt, *Geophysical Journal International*, **165**, 705-718.

Mora, P., 1987. Nonlinear two-dimensional elastic inversion of multioffset seismic data, *Geophysics*, **52**, 1211-1228.

Müller, K., Vanderborght, J., Englert, A., Kemna, A., Huisman, J. A., et al., 2010. Imaging and characterization of solute transport during two tracer tests in a shallow aquifer using electrical resistivity tomography and multilevel groundwater samplers, *Water Resources Research*, **46**, W03502.

Musil, M., Maurer, H. R., and Green, A. G., 2003. Discrete tomography and joint inversion for loosely connected or unconnected physical properties: Application to crosshole seismic and georadar data sets, *Geophysical Journal International*, **153**, 389-402.

Nadeau, D. F., Brutsaert, W., Parlange, M. B., Bou-Zeid, E., Barrenetxea, G., et al., 2009. Estimation of urban sensible heat flux using a dense wireless network of observations, *Environmental Fluid Mechanics*, **9**, 635-653.

Nimmer, R. E., Osiensky, J. L., Binley, A. M., Sprenke, K. F., and Williams, B. C., 2007. Electrical resistivity imaging of conductive plume dilution in fractured rock, *Hydrogeology Journal*, **15**, 877-890.

Nimmer, R. E., Osiensky, J. L., Binley, A. M., and Williams, B. C., 2008. Three-dimensional effects causing artifacts in two-dimensional, cross-borehole, electrical imaging, *Journal of Hydrology*, **359**, 59-70.

Nyquist, J. E., Freyer, P. A., and Toran, L., 2008. Stream bottom resistivity tomography to map ground water discharge, *Ground Water*, **46**, 561-569.

Ogilvy, R. D., Meldrum, P. I., Kuras, O., Wilkinson, P. B., Chambers, J. E., et al., 2009. Automated monitoring of coastal aquifers with electrical resistivity tomography, *Near Surface Geophysics*, **7**, 367-375.

Oldenburg, D. W., and Li, Y. G., 1999. Estimating depth of investigation in dc resistivity and IP surveys, *Geophysics*, **64**, 403-416.

Olsson, O., Falk, L., Forslund, O., Lundmark, L., and Sandberg, E., 1992. Borehole radar applied to the characterization of hydraulically conductive fracture-zones in crystalline rock, *Geophysical Prospecting*, **40**, 109-142.

Oreskes, N., Shrader-Frechette, K., and Belitz, K., 1994. Verification, validation, and confirmation of numerical models in the earth sciences, *Science*, **263**, 641-646.

Orghidan, T., 1959. Ein neuer Lebensraum des unterirdischen Wassers: der hyporheische Biotop, *Arch. Hydrobiol.*, **55**, 392-414.

Osiensky, J. L., Nimmer, R., and Binley, A. M., 2004. Borehole cylindrical noise during hole-surface and hole-hole resistivity measurements, *Journal of Hydrology*, **289**, 78-94.

Paasche, H., Tronicke, J., Holliger, K., Green, A. G., and Maurer, H., 2006. Integration of diverse physical-property models: Subsurface zonation and petrophysical parameter estimation based on fuzzy c-means cluster analyses, *Geophysics*, **71**, H33-H44.

Paasche, H., and Tronicke, J., 2007. Cooperative inversion of 2D geophysical data sets: A zonal approach based on fuzzy c-means cluster analysis, *Geophysics*, **72**, A35-A39.

Paasche, H., Wendrich, A., Tronicke, J., and Trela, C., 2008. Detecting voids in masonry by cooperatively inverting P-wave and georadar traveltimes, *Journal of Geophysics and Engineering*, **5**, 256-267.

Paige, C. C., and Saunders, M. A., 1982. LSQR: An algorithm for sparse linear equations and sparse least squares, *ACM Transactions on Mathematical Software*, **8**, 43-71.

Palmer, M. A., Bernhardt, E. S., Allan, J. D., Lake, P. S., Alexander, G., et al., 2005. Standards for ecologically successful river restoration, *Journal of Applied Ecology*, **42**, 208-217.

Park, S. K., Johnston, M. J. S., Madden, T. R., Morgan, F. D., and Morrison, H. F., 1993. Electromagnetic precursors to earthquakes in the ULF band - a review of observations and mechanisms, *Reviews of Geophysics*, **31**, 117-132.

Parker, R. L., 1984. The inverse problem of resistivity sounding, *Geophysics*, **49**, 2143-2158.

Pasquale, N., Perona, P., Schneider, P., Shrestha, J., Wombacher, A., and Burlando, P., 2011. Modern comprehensive approach to monitor the morphodynamic evolution of a restored river corridor, *Hydrology and Earth System Sciences*, **15**, 1197-1212.

Perrier, F., and Morat, P., 2000. Characterization of electrical daily variations induced by capillary flow in the non-saturated zone, *Pure and Applied Geophysics*, **157**, 785-810.

Petiau, G., 2000. Second generation of lead-lead chloride electrodes for geophysical applications, *Pure and Applied Geophysics*, **157**, 357-382.

Podvin, P., and Lecomte, I., 1991. Finite difference computation of traveltimes in very contrasted velocity models: A massively parallel approach and its associated tools, *Geophysical Journal International*, **105**, 271-284.

Pollock, D., and Cirpka, O. A., 2010. Fully coupled hydrogeophysical inversion of synthetic salt tracer experiments, *Water Resources Research*, **46**, W07501.

Portniaguine, O., and Zhdanov, M. S., 1999. Focusing geophysical inversion images, *Geophysics*, **64**, 874-887.

Pratt, R. G., 1999. Seismic waveform inversion in the frequency domain, part 1: Theory and verification in a physical scale model, *Geophysics*, **64**, 888-901.

Pratt, R. G., and Shipp, R. M., 1999. Seismic waveform inversion in the frequency domain, part 2: Fault delineation in sediments using crosshole data, *Geophysics*, **64**, 902-914.

Pride, S., 1994. Governing equations for the coupled electromagnetics and acoustics of porous-media, *Physical Review B*, **50**, 15678-15696.

Pride, S. R., Berryman, J. G., and Harris, J. M., 2004. Seismic attenuation due to wave-induced flow, *Journal of Geophysical Research-Solid Earth*, **109**, B01201.

Pruess, K., Oldenburg, C. M., and Moridis, G. J., 1999. TOUGH2 user's guide version 2, Rep. LBNL--43134, 204 pp, Lawrence Berkeley National Laboratory.

Ptak, T., and Teutsch, G., 1994. Forced and natural gradient tracer tests in a highly heterogeneous porous aquifer - instrumentation and measurements, *Journal of Hydrology*, **159**, 79-104.

Ramirez, A., Daily, W., Labrecque, D., Owen, E., and Chesnut, D., 1993. Monitoring an underground steam injection process using electrical-resistance tomography, *Water Resources Research*, **29**, 73-87.

Ranguelova, E. B., 2002. *Segmentation of textured images on three-dimensional lattices*: PhD thesis, University of Dublin.

RECORD, 2011. Assessment and modeling of coupled ecological and hydrological dynamics in the restored corridor of the river, *Competence Center Environment and Sustainability*, http://www.cces.ethz.ch/projects/nature/Record.

Regli, C., Rauber, M., and Huggenberger, P., 2003. Analysis of aquifer heterogeneity within a well capture zone, comparison of model data with field experiments: A case study from the river Wiese, Switzerland, *Aquatic Sciences*, **65**, 111-128.

Revil, A., Cathles, L. M., Losh, S., and Nunn, J. A., 1998. Electrical conductivity in shaly sands with geophysical applications, *Journal of Geophysical Research - Solid Earth*, **103**, 23925-23936.

Revil, A., and Cathles, L. M., 1999. Permeability of shaly sands, *Water Resources Research*, **35**, 651-662.

Revil, A., Naudet, V., Nouzaret, J., and Pessel, M., 2003. Principles of electrography applied to self-potential electrokinetic sources and hydrogeological applications, *Water Resources Research*, **39**, 1114.

Revil, A., and Leroy, P., 2004. Constitutive equations for ionic transport in porous shales, *Journal of Geophysical Research-Solid Earth*, **109**, B03208.

Revil, A., and Linde, N., 2006. Chemico-electromechanical coupling in microporous media, *Journal of Colloid and Interface Science*, **302**, 682-694.

Revil, A., Linde, N., Cerepi, A., Jougnot, D., Matthai, S., and Finsterle, S., 2007. Electrokinetic coupling in unsaturated porous media, *Journal of Colloid and Interface Science*, **313**, 315-327.

Revil, A., Trolard, F., Bourrie, G., Castermant, J., Jardani, A., and Mendonca, C. A., 2009. Ionic contribution to the self-potential signals associated with a redox front, *Journal of Contaminant Hydrology*, **109**, 27-39.

Rizzo, E., Suski, B., Revil, A., Straface, S., and Troisi, S., 2004. Self-potential signals associated with pumping tests experiments, *Journal of Geophysical Research-Solid Earth*, **109**, B10203.

Robinson, D. A., Binley, A., Crook, N., Day-Lewis, F. D., Ferre, T. P. A., et al., 2008. Advancing process-based watershed hydrological research using near-surface geophysics: A vision for, and review of, electrical and magnetic geophysical methods, *Hydrological Processes*, **22**, 3604-3635.

Rubin, Y., and Hubbard, S. S. (Eds.), 2005. *Hydrogeophysics*, Springer, Dordrecht, The Netherlands.

Rücker, C., Günther, T., and Spitzer, K., 2006. Three-dimensional modelling and inversion of dc resistivity data incorporating topography - I. Modelling, *Geophysical Journal International*, **166**, 495-505.

Ruelleu, S., Moreau, F., Bour, O., Gapais, D., and Martelet, G., 2010. Impact of gently dipping discontinuities on basement aquifer recharge: An example from Ploemeur (Brittany, France), *Journal of Applied Geophysics*, **70**, 161-168.

Samaritani, E., Shrestha, J., Fournier, B., Frossard, E., Gillet, F., et al., 2011. Heterogeneity of soil carbon pools and fluxes in a channelized and a restored floodplain section (Thur River, Switzerland), *Hydrology and Earth System Sciences Discussions*, **8**, 1059-1091.

Sambridge, M., Braun, J., and Mcqueen, H., 1995. Geophysical parametrization and interpolation of irregular data using natural neighbors, *Geophysical Journal International*, **122**, 837-857.

Sandberg, S. K., Slater, L. D., and Versteeg, R., 2002. An integrated geophysical investigation of the hydrogeology of an anisotropic unconfined aquifer, *Journal of Hydrology*, **267**, 227-243.

Saracco, G., Labazuy, P., and Moreau, F., 2004. Localization of self-potential sources in volcano-electric effect with complex continuous wavelet transform and electrical tomography methods for an active volcano, *Geophysical Research Letters*, **31**, L12610.

Schälchli, U., 1992. The clogging of coarse gravel river beds by fine sediment, *Hydrobiologia*, **235-236**, 189-197.

Schälchli, U., 2008. Geschiebehaushalt im Thurgebiet, *Wasser Energie Luft*, **100**, 23-28.

Schäppi, B., Perona, P., Schneider, P., and Burlando, P., 2010. Integrating river cross section measurements with digital terrain models for improved flow modelling applications, *Computers & Geosciences*, **36**, 707-716.

Scheibe, T. D., and Chien, Y. J., 2003. An evaluation of conditioning data for solute transport prediction, *Ground Water*, **41**, 128-141.

Schmidt, C., Bayer-Raich, M., and Schirmer, M., 2006. Characterization of spatial heterogeneity of groundwater-stream water interactions using multiple depth streambed temperature measurements at the reach scale, *Hydrology and Earth System Sciences*, **10**, 849-859.

Schmidt, C., Conant, B., Bayer-Raich, M., and Schirmer, M., 2007. Evaluation and field-scale application of an analytical method to quantify groundwater discharge using mapped streambed temperatures, *Journal of Hydrology*, **347**, 292-307.

Schneider, P., Vogt, T., Schirmer, M., Doetsch, J., Linde, N., et al., 2011. Towards improved instrumentation for assessing river-groundwater interactions in a restored river corridor, *Hydrology and Earth System Sciences*, **15**, 2531-2549.

Schön, J. H., 1996. *Physical properties of rocks: Fundamentals and principles of petrophysics*, Elsevier Science Publishing Company, Inc.

Schulmeister, M. K., Butler, J. J., Healey, J. M., Zheng, L., Wysocki, D. A., and McCall, G. W., 2003. Direct-push electrical conductivity logging for high-resolution hydrostratigraphic characterization, *Ground Water Monitoring and Remediation*, **23**, 52-62.

Schwarzenbach, R. P., and Westall, J., 1981. Transport of non-polar organic-compounds from surface-water to groundwater - Laboratory sorption studies, *Environmental Science & Technology*, **15**, 1360-1367.

Schwarzenbach, R. P., Giger, W., Hoehn, E., and Schneider, J. K., 1983. Behavior of organic-compounds during infiltration of river water to groundwater - Field studies, *Environmental Science & Technology*, **17**, 472-479.

Schwarzenbach, R. P., Escher, B. I., Fenner, K., Hofstetter, T. B., Johnson, C. A., et al., 2006. The challenge of micropollutants in aquatic systems, *Science*, **313**, 1072-1077.

Seiz, G., and Foppa, N., 2007. Nationales Klima-Beobachtungssystem (GCOS Schweiz), *Bundesamt für Meteorologie und Klimatologie, MeteoSchweiz und ProClim, Bern, Switzerland*.

Selker, J. S., Thevenaz, L., Huwald, H., Mallet, A., Luxemburg, W., et al., 2006. Distributed fiber-optic temperature sensing for hydrologic systems, *Water Resources Research*, **42**, W12202.

Sen, P. N., Scala, C., and Cohen, M. H., 1981. A self-similar model for sedimentary-rocks with application to the dielectric-constant of fused glass-beads, *Geophysics*, **46**, 781-795.

Shankar, V., Eckert, P., Ojha, C. S. P., and Konig, C. M., 2009. Transient three-dimensional modeling of riverbank filtration at Grind well field, Germany, *Hydrogeology Journal*, **17**, 321-326.

Sheffer, M. R., and Oldenburg, D. W., 2007. Three-dimensional modelling of streaming potential, *Geophysical Journal International*, **169**, 839-848.

Sill, W. R., 1983. Self-potential modeling from primary flows, *Geophysics*, **48**, 76-86.

Silliman, S. E., and Booth, D. F., 1993. Analysis of time-series measurements of sediment temperature for identification of gaining vs losing portions of Juday-Creek, Indiana, *Journal of Hydrology*, **146**, 131-148.

Singha, K., and Gorelick, S. M., 2005. Saline tracer visualized with three-dimensional electrical resistivity tomography: Field-scale spatial moment analysis, *Water Resources Research*, **41**, W05023.

Sjödahl, P., Dahlin, T., and Johansson, S., 2009. Embankment dam seepage evaluation from resistivity monitoring data, *Near Surface Geophysics*, **7**, 463-474.

Slater, L., and Sandberg, S. K., 2000. Resistivity and induced polarization monitoring of salt transport under natural hydraulic gradients, *Geophysics*, **65**, 408-420.

Slater, L., Binley, A. M., Daily, W., and Johnson, R., 2000. Cross-hole electrical imaging of a controlled saline tracer injection, *Journal of Applied Geophysics*, **44**, 85-102.

Slater, L., and Binley, A., 2006. Synthetic and field-based electrical imaging of a zerovalent iron barrier: Implications for monitoring long-term barrier performance, *Geophysics*, **71**, B129-B137.

Slob, E., Sato, M., and Olhoeft, G., 2010. Surface and borehole ground-penetrating-radar developments, *Geophysics*, **75**, A103-A120.

Smith, D. G., and Jol, H. M., 1992. Ground-penetrating radar investigation of a Lake Bonneville delta, Provo level, Brigham City, Utah, *Geology*, **20**, 1083-1086.

Soar, P. J., and Thorne, C. R., 2001. *Channel restoration design for meandering rivers*, U.S. Army Engineer Research and Development Center, Vicksburg, Miss.

Spillmann, T., Maurer, H., Willenberg, H., Evans, K. F., Heincke, B., and Green, A. G., 2007. Characterization of an unstable rock mass based on borehole logs and diverse borehole radar data, *Journal of Applied Geophysics*, **61**, 16-38.

Springer, R. K., and Gelhar, L. W., 1991. Characterization of large-scale aquifer heterogeneity in glacial outwash by analysis of slug tests with oscillatory response, *US Geological Survey, Cape Cod*, Report 91-4034.

Stanford, J. A., and Ward, J. V., 1988. The hyporheic habitat of river ecosystems, *Nature*, **335**, 64-66.

Stanford, J. A., and Ward, J. V., 1993. An ecosystem perspective of alluvial rivers - connectivity and the hyporheic corridor, *Journal of the North American Benthological Society*, **12**, 48-60.

Stauffer, F., and Dracos, T., 1986. Experimental and numerical study of water and solute infiltration in layered porous-media, *Journal of Hydrology*, **84**, 9-34.

Storey, R. G., Howard, K. W. F., and Williams, D. D., 2003. Factors controlling riffle-scale hyporheic exchange flows and their seasonal changes in a gaining stream: A three-dimensional groundwater flow model, *Water Resources Research*, **39**, 1034.

Streich, R., van der Kruk, J., and Green, A. G., 2006. Three-dimensional multicomponent georadar imaging of sedimentary structures, *Near Surface Geophysics*, **4**, 39-48.

Streich, R., and van der Kruk, J., 2007a. Accurate imaging of multicomponent GPR data based on exact radiation patterns, *Ieee Transactions on Geoscience and Remote Sensing*, **45**, 93-103.

Streich, R., and van der Kruk, J., 2007b. Characterizing a GPR antenna system by near-field electric field measurements, *Geophysics*, **72**, A51-A55.

Stummer, P., Maurer, H., and Green, A. G., 2004. Experimental design: Electrical resistivity data sets that provide optimum subsurface information, *Geophysics*, **69**, 120-139.

Suski, B., Revil, A., Titov, K., Konosavsky, P., Voltz, M., et al., 2006. Monitoring of an infiltration experiment using the self-potential method, *Water Resources Research*, **42**, W08418.

SVGW, 2004. Jahrbuch 2003/2004, *SVGW, Zürich*.

SVGW, 2007. Empfehlungen – Revitalisierung im Einflussbereich von Trinkwasserfassungen, *Zürich, Switzerland*.

Talley, J., Baker, G. S., Becker, M. W., and Beyrle, N., 2005. Four dimensional mapping of tracer channelization in subhorizontal bedrock fractures using surface ground penetrating radar, *Geophysical Research Letters*, **32**, L04401.

Tarantola, A., 1984a. Inversion of seismic-reflection data in the acoustic approximation, *Geophysics*, **49**, 1259-1266.

Tarantola, A., 1984b. Linearized inversion of seismic-reflection data, *Geophysical Prospecting*, **32**, 998-1015.

Tarantola, A., 1986. A strategy for nonlinear elastic inversion of seismic-reflection data, *Geophysics*, **51**, 1893-1903.

Thony, J. L., Morat, P., Vachaud, G., and LeMouel, J. L., 1997. Field characterization of the relationship between electrical potential gradients and soil water flux, *Comptes Rendus De L'Academie Des Sciences*, **325**, 317-321.

Topp, G. C., Davis, J. L., and Annan, A. P., 1980. Electromagnetic determination of soil-water content - Measurements in coaxial transmission-lines, *Water Resources Research*, **16**, 574-582.

Topp, G. C., Davis, J. L., and Annan, A. P., 1982. Electromagnetic determination of soil-water content using TDR 2. Evaluation of installation and configuration of parallel transmission-lines, *Soil Science Society of America Journal*, **46**, 678-684.

Torrence, C., and Compo, G. P., 1998. A practical guide to wavelet analysis, *Bulletin of the American Meteorological Society*, **79**, 61-78.

Touchard, F., 1999. *Caractérisation hydrogéologique d'un aquifère en socle fracture. Site de Ploëmeur (Morbihan)*: PhD thesis, University of Rennes I.

Trefry, M. G., and Muffels, C., 2007. Feflow: A finite-element ground water flow and transport modeling tool, *Ground Water*, **45**, 525-528.

Triska, F. J., Kennedy, V. C., Avanzino, R. J., Zellweger, G. W., and Bencala, K. E., 1989. Retention and transport of nutrients in a 3rd-order stream in Northwestern California - hyporheic processes, *Ecology*, **70**, 1893-1905.

Triska, F. J., Duff, J. H., and Avanzino, R. J., 1993a. Patterns of hydrological exchange and nutrient transformation in the hyporheic zone of a gravel-bottom stream - examining terrestrial aquatic linkages, *Freshwater Biology*, **29**, 259-274.

Triska, F. J., Duff, J. H., and Avanzino, R. J., 1993b. The role of water exchange between a stream channel and its hyporheic zone in nitrogen cycling at the terrestrial aquatic interface, *Hydrobiologia*, **251**, 167-184.

Tronicke, J., Dietrich, P., Wahlig, U., and Appel, E., 2002. Integrating surface georadar and crosshole radar tomography: A validation experiment in braided stream deposits, *Geophysics*, **67**, 1516-1523.

Tronicke, J., and Holliger, K., 2004. Effects of gas- and water-filled boreholes on the amplitudes of crosshole georadar data as inferred from experimental evidence, *Geophysics*, **69**, 1255-1260.

Tronicke, J., Holliger, K., Barrash, W., and Knoll, M. D., 2004. Multivariate analysis of cross-hole georadar velocity and attenuation tomograms for aquifer zonation, *Water Resources Research*, **40**, W01519.

Trubilowicz, J., Cai, K., and Weiler, M., 2009. Viability of motes for hydrological measurement, *Water Resources Research*, **45**, W00D22.

Trush, W. J., McBain, S. M., and Leopold, L. B., 2000. Attributes of an alluvial river and their relation to water policy and management, *Proceedings of the National Academy of Sciences of the United States of America*, **97**, 11858-11863.

Tryggvason, A., Rögnvaldsson, S. T., and Flóvenz, Ó. G., 2002. Three-dimensional imaging of the P- and S-wave velocity structure and earthquake locations beneath Southwest Iceland, *Geophysical Journal International*, **151**, 848-866.

Tryggvason, A., and Linde, N., 2006. Local earthquake (LE) tomography with joint inversion for P- and S-wave velocities using structural constraints, *Geophysical Research Letters*, **33**, L07303.

Tryggvason, A., and Bergman, B., 2006. A traveltime reciprocity discrepancy in the Podvin & Lecomte time3d finite difference algorithm, *Geophysical Journal International*, **165**, 432-435.

Tsoflias, G. P., Halihan, T., and Sharp, J. M., 2001. Monitoring pumping test response in a fractured aquifer using ground-penetrating radar, *Water Resources Research*, **37**, 1221-1229.

Tsoflias, G. P., and Becker, M. W., 2008. Ground-penetrating-radar response to fracture-fluid salinity: Why lower frequencies are favorable for resolving salinity changes, *Geophysics*, **73**, J25-J30.

Tubino, M., and Seminara, G., 1990. Free forced interactions in developing meanders and suppression of free bars, *Journal of Fluid Mechanics*, **214**, 131-159.

Tufenkji, N., Ryan, J. N., and Elimelech, M., 2002. The promise of bank filtration, *Environmental Science & Technology*, **36**, 422A-428A.

Turesson, A., 2006. Water content and porosity estimated from ground-penetrating radar and resistivity, *Journal of Applied Geophysics*, **58**, 99-111.

van Genuchten, M. T., 1980. A closed-form equation for predicting the hydraulic conductivity of unsaturated soils, *Soil Science Society of America Journal*, **44**, 892-898.

Vasco, D. W., Peterson, J. E., and Majer, E. L., 1995. Beyond ray tomography - Wavepaths and fresnel volumes, *Geophysics*, **60**, 1790-1804.

Vereecken, H., Binley, A., Cassiani, G., Revil, A., and Titov, K. (Eds.), 2006. *Applied hydrogeophysics*, Springer, Dordrecht, The Netherlands.

Vereecken, H., Huisman, J. A., Bogena, H., Vanderborght, J., Vrugt, J. A., and Hopmans, J. W., 2008. On the value of soil moisture measurements in vadose zone hydrology: A review, *Water Resources Research*, **44**, W00D06.

Vogt, T., Hoehn, E., Schneider, P., and Cirpka, O. A., 2009. Untersuchung der Flusswasserinfiltration in voralpinen Schottern mittels Zeitreihenanalyse, *Grundwasser*, **14**, 179-194.

Vogt, T., Schneider, P., Hahn-Woernle, L., and Cirpka, O. A., 2010a. Estimation of seepage rates in a losing stream by means of fiber-optic high-resolution vertical temperature profiling, *Journal of Hydrology*, **380**, 154-164.

Vogt, T., Hoehn, E., Schneider, P., Freund, A., Schirmer, M., and Cirpka, O. A., 2010b. Fluctuations of electrical conductivity as a natural tracer for bank filtration in a losing stream, *Advances in Water Resources*, **33**, 1296-1308.

von Gunten, H. R., Karametaxas, G., and Keil, R., 1994. Chemical Processes in Infiltrated Riverbed Sediments, *Environmental Science & Technology*, **28**, 2087-2093.

von Gunten, U., and Zobrist, J., 1993. Biogeochemical changes in groundwater-infiltration systems - column studies, *Geochimica Et Cosmochimica Acta*, **57**, 3895-3906.

Vozoff, K., and Jupp, D. L. B., 1975. Joint inversion of geophysical data, *Geophysical Journal of the Royal Astronomical Society*, **42**, 977-991.

Ward, A. S., Gooseff, M. N., and Singha, K., 2010. Imaging hyporheic zone solute transport using electrical resistivity, *Hydrological Processes*, **24**, 948-953.

Ward, J. V., 1989. The four-dimensional nature of lotic ecosystems, *Journal of the North American Benthological Society*, **8**, 2-8.

Watanabe, T., Nihei, K. T., Nakagawa, S., and Myer, L. R., 2004. Viscoacoustic wave form inversion of transmission data for velocity and attenuation, *Journal of the Acoustical Society of America*, **115**, 3059-3067.

Waxman, M. H., and Smits, L. J. M., 1968. Electrical Conductivities in Oil-Bearing Shaly Sands, *Society of Petroleum Engineers Journal*, **8**, 107.

West, L. J., Handley, K., Huang, Y., and Pokar, M., 2003. Radar frequency dielectric dispersion in sandstone: Implications for determination of moisture and clay content, *Water Resources Research*, **39**, 1026.

Western, A. W., Grayson, R. B., and Blöschl, G., 2002. Scaling of soil moisture: A hydrologic perspective, *Annual Review of Earth and Planetary Sciences*, **30**, 149-180.

Wilkinson, P. B., Meldrum, P. I., Kuras, O., Chambers, J. E., Holyoake, S. J., and Ogilvy, R. D., 2010. High-resolution electrical resistivity tomography monitoring of a tracer test in a confined aquifer, *Journal of Applied Geophysics*, **70**, 268-276.

Winship, P., Binley, A., and Gomez, D., 2006. Flow and transport in the unsaturated Sherwood Sandstone: Characterization using cross-borehole geophysical methods, *Fluid Flow and Solute Movement in Sandstones: The Onshore UK Permo-Triassic Red Bed Sequence*, **263**, 219-231.

Wishart, D. N., Slater, L. D., and Gates, A. E., 2006. Self potential improves characterization of hydraulically-active fractures from azimuthal geoelectrical measurements, *Geophysical Research Letters*, **33**, L17314.

Woessner, W. W., 2000. Stream and fluvial plain ground water interactions: Rescaling hydrogeologic thought, *Ground Water*, **38**, 423-429.

Wombacher, A., and Schneider, P., 2010. Observation centric sensor data model, *Technical Report TR-CTIT-10-13, University of Twente, Enschede*, ISSN 1381-3625.

Woolsey, S., Capelli, F., Gonser, T., Hoehn, E., Hostmann, M., et al., 2007. A strategy to assess river restoration success, *Freshwater Biology*, **52**, 752-769.

Worthington, P. F., 1993. The uses and abuses of the archie equations 1. The formation factor porosity relationship, *Journal of Applied Geophysics*, **30**, 215-228.

Wriedt, G., and Rode, M., 2006. Modelling nitrate transport and turnover in a lowland catchment system, *Journal of Hydrology*, **328**, 157-176.

Wroblicky, G. J., Campana, M. E., Valett, H. M., and Dahm, C. N., 1998. Seasonal variation in surface-subsurface water exchange and lateral hyporheic area of two stream-aquifer systems, *Water Resources Research*, **34**, 317-328.

Yeh, T. C. J., Liu, S., Glass, R. J., Baker, K., Brainard, J. R., et al., 2002. A geostatistically based inverse model for electrical resistivity surveys and its applications to vadose zone hydrology, *Water Resources Research*, **38**, 1278.

Yeh, T. C. J., Lee, C. H., Hsu, K. C., Illman, W. A., Barrash, W., et al., 2008. A view toward the future of subsurface characterization: CAT scanning groundwater basins, *Water Resources Research*, **44**, W03301.

Yilmaz, Ö., 2001. *Seismic data processing*, Society of Exploration Geophysicists, Tulsa, USA.

Zhang, J., and Morgan, F. D., 1997. Joint Seismic and Electrical Tomography, *Proceedings of the Symposium on the Application of Geophysics to Engineering and Environmental Problems*, 391-396.

Zhdanov, M. S., 2009. New advances in regularized inversion of gravity and electromagnetic data, *Geophysical Prospecting*, **57**, 463-478.

Zhou, B., and Greenhalgh, S. A., 2003. Crosshole seismic inversion with normalized full-waveform amplitude data, *Geophysics*, **68**, 1320-1330.

Zonge, K., Wynn, J., and Urquhart, S., 2005. Resistivity, induced polarization, and complex resistivity, in *Near Surface Geophysics*, edited by D. K. Butler, pp. 265-300, SEG.

Zurbuchen, B. R., Zlotnik, V. A., and Butler, J. J., 2002. Dynamic interpretation of slug tests in highly permeable aquifers, *Water Resources Research*, **38**, 1025.